Abstract

Quantum phases and transitions of many-body systems realized using cold atomic gases

Stephen Christopher Powell

2007

In recent years, new advances in techniques for trapping and cooling atoms have allowed the production of atomic gases at low-enough temperatures and high-enough densities for collective quantum-mechanical effects to become important. This thesis describes theoretical investigations of certain many-body physics problems motivated by these experimental developments. It consists of two main parts.

In the first, I investigate the array of phases exhibited by degenerate mixtures of bosons and fermions with a Feshbach resonance, a bound molecular state whose energy can be tuned with a magnetic field. These phases are distinguished by the presence or absence of a bosonic condensate and also by the different Luttinger constraints that are shown to apply to the Fermi surface(s).

The second part is concerned with bosons in an optical lattice, in which a periodic potential is produced by counterpropagating lasers. Spinless bosons are known to exhibit a quantum phase transition between a Mott insulator and a superfluid state, while bosons with spin have a much richer phase structure. I consider, in particular, a phase transition with a spinless order parameter, and show that the long-time dynamics of spin-carrying excitations is governed by a nontrivial fixed point. The corresponding anomalous exponents are found using a renormalization-group calculation.

Quantum phases and transitions of many-body systems realized using cold atomic gases

A Dissertation
Presented to the Faculty of the Graduate School
of
Yale University
in Candidacy for the Degree of
Doctor of Philosophy

by
Stephen Christopher Powell

Dissertation Director: Ramamurti Shankar

May 2007

Contents

Acknowledgments

First and foremost, I thank Subir Sachdev, who acted as my research adviser and coauthored the two articles that this thesis is based upon. I also thank Ramamurti Shankar, who took over the reins after Subir's departure. Both provided plenty of useful advice on matters of research and much else besides.

I am also deeply indebted to the other members of my dissertation committee, Steve Girvin, Dave DeMille and Jack Harris, whose insightful questioning helped to clarify several important points.

I am very grateful to Hans Peter Büchler, who was a coauthor of one of the two articles, and to Krishnendu Sengupta, with whom I discussed many aspects of the research. I also thank, amongst others, Mara Baraban, Lorentz Bartosch, Lev Bishop, Jack Challis, Adrian Del Maestro, Tom Jackson, George Mias, and Terri Yu, for help and encouragement during my time in the Yale physics department.

I acknowledge financial support from the National Science Foundation and the William C. G. Ortel Fellowship in Physics.

Finally, many thanks to Michael, Judy and Shialing for their unwavering support throughout.

List of Figures

Chapter 1

Introduction

The behavior of physical systems with many constituent parts interacting strongly with each other has long been a central concern in the theory of condensed matter. It is only within roughly the past decade that it has been possible to produce gases of atoms at sufficiently high density and low temperature that the effects of their mutual interactions become significant. These systems, while interesting in their own right, also provide a useful toolbox for the study of many-body physics in other contexts. This thesis will describe theoretical studies of two examples of such systems.

The recent growth of interest in many-body phenomena in atomic systems was started by the realization, in 1995, of a Bose-Einstein condensate (BEC) in an 'ultracold' gas of rubidium atoms [1]. Bose-Einstein condensation, predicted in 1924 [2–4], refers to the macroscopic occupation of a single quantum state [5, 6]. It was recognized as the cause of superfluidity in liquid helium as early as 1938 [7, 8], but strong interactions in that system made quantitative comparisons with theory difficult [9].

There are several attractive features of ultracold atomic gases that have caused them to be the focus of particular interest. An immediate advantage of the atomic BEC was that the relatively weak interactions allowed for more direct comparison

with the theory of weakly interacting bosons [10, 11].

A second advantage is the ability to observe condensation directly by probing the momentum-space distribution of the atoms. In a typical experiment, the atoms are trapped within a tight optical or magnetic potential [12, 13], and then suddenly released, by rapidly switching off the potential [1]. Using the 'sudden approximation' [14], the atoms are projected onto momentum states, and subsequently evolve essentially independently [15]. After a certain 'time of flight' has elapsed, the spatial density profile of the cloud is measured (for example, via the optical density for absorption) which, assuming free propagation after the trap is released, gives a direct measurement of the momentum-space distribution prior to release. Bose-Einstein condensation is then signaled by the appearance of a sharp peak near zero momentum, superimposed upon the thermal distribution [1]. It is also possible to measure correlations in the momentum distribution, as a means to identify quantum states with nontrivial correlations [15].

A third advantage, the extent to which their properties can be controlled and modified in experiments, has led to the development of a vast array of new experimental techniques, motivated, in large part, by the goal of simulating various systems of interest in solid-state physics [16–19]. In the remainder of this chapter, I will give a brief description of some of these techniques and the theoretical models that have been used to describe them.

1.1 Feshbach resonance

The Feshbach resonance [20–22], which originated in nuclear physics and was first demonstrated in an atomic context by Inouye *et al.* [23], has emerged as a useful technique for forming bound states of neutral atoms. The term refers to a molecular

state whose binding energy can be 'tuned' by varying an external parameter. For example, by choosing a bound state with a different magnetic moment from the unbound atoms, the relative energy of the resonance can be changed with an external magnetic field [23, 24].

A simple model Hamiltonian can be written as [25]

$$\mathcal{H} = \int \mathrm{d}^d\mathbf{x} \Bigg\{ \sum_{\sigma\in\{1,2\}} \psi_\sigma^\dagger \left(-\frac{\nabla^2}{2m_\sigma} - \mu_\sigma \right) \psi_\sigma + \Psi^\dagger \left[-\frac{\nabla^2}{2(m_1+m_2)} - (\mu_1+\mu_2) + \nu \right] \Psi + g\left(\Psi^\dagger \psi_1 \psi_2 + \psi_2^\dagger \psi_1^\dagger \Psi \right) \Bigg\}, \quad (1.1)$$

where ψ_σ is the field (annihilation) operator for atomic species[1] σ, m_σ and μ_σ are the corresponding mass and chemical potential, and Ψ is the field operator for the molecular state. The energy of the bound state relative to the two-atom continuum is denoted ν and referred to as the detuning.

The final term in $\mathcal{H}$ represents the physical process where two atoms combine to form a molecule, as well as its opposite. Interactions other than this pairing term are assumed to be less important near resonance and have been omitted.

One effect of the Feshbach resonance is to alter the scattering properties for the atomic species. For $\nu \approx 0$, the scattering length a between the two atoms is dominated by the presence of the bound state Ψ [26]. Sufficiently close to the resonance, a is inversely proportional to ν [22], so that the strength of the interaction can be adjusted over a wide range of values, both attractive and repulsive. The enhanced scattering near resonance can be viewed as resulting from virtual transitions into the molecular state.

The presence of the molecular state also allows for new and interesting many-

[1] For bosonic atoms, the two atoms may be of the same species, in which case the index σ should be ignored throughout.

body phases, with various possibilities depending on the quantum statistics of the atomic species.

If both atoms are fermions, the molecular species Ψ is a boson, and a BEC of molecules is formed at low temperature [27–29], provided ν is not too large. For $\nu \gg 0$, where formation of molecules is unfavorable, the system crosses over into a state of paired fermions [30], analogous to the BCS phenomenon in metals [31]. The 'BCS–BEC crossover' between these regimes has been the subject of particular interest, both experimental [32,33] and theoretical [34,35]. (For a recent review, see Ref. [36].)

The case of a Feshbach resonance between two atoms of the same species of bosons has also been considered [37,38]. In this case, a BEC of individual atoms is possible for $\nu \gg 0$, while a BEC of molecules again forms for $\nu \ll 0$. Unlike the fermionic case, these two states cannot be connected smoothly to each other[2] and a quantum phase transition between the two occurs at some value of ν [37,38].

The third possibility, a Feshbach resonance between a fermion and a boson, has been observed experimentally by several groups [39–41]. Chapter 2 will consider this case in some detail, and show that various phases are possible, distinguished by the presence or absence of an atomic BEC, and the number of Fermi surfaces. Observing these phases in experiment requires simultaneous degeneracy of both atomic species [42,43] and of the molecule. In Section 4.1, we describe some recent experimental developments in this direction.

A purely optical Feshbach resonance has also been predicted [44] and observed [45]. This allows rotation symmetry to be preserved and hence the manipulation of

[2]This can mostly easily be seen by considering the symmetries that are broken in the two cases. There is a U(1) symmetry operation of $\mathcal{H}$ under which $\psi \to \psi e^{i\theta}$ and $\Psi \to \Psi e^{2i\theta}$, corresponding to the conservation of the total number of atoms. A BEC of atoms, $\langle\psi\rangle \neq 0$, breaks this symmetry completely, whereas with only a BEC of molecules, $\langle\Psi\rangle \neq 0$, the special case of $\theta = \pi$ remains as an unbroken Z_2 symmetry. This distinguishes the two cases qualitatively and shows that they must be divided by a phase transition at which the Z_2 symmetry is broken [37,38].

multiple spin species, as described below in Section 1.3.

1.2 Optical lattices

A parallel experimental advance, of great significance from the point of view of simulation of solid-state systems, has been the development of optical lattices [46–49].

Laser trapping uses the effective potential produced by the AC Stark effect [50] to confine atoms, which are attracted to maxima or minima of the intensity (with red- or blue-detuned light, respectively). By using a pair of counterpropagating laser beams, it is possible to set up a standing light wave; using three such pairs, a three-dimensional periodic lattice potential can be produced.

This allows for unprecedented control over the parameters of the lattice: the depth of the potential is determined by the intensity of the light and the lattice constant by its wavelength. By making the intensity in the three directions highly anisotropic, the lattice can be made effectively one- or two-dimensional. Besides simple square and cubic lattices, it is possible to produce more complicated structures by appropriate choice of the relative phases and directions of the lasers. (See, for instance, Ref. [51], which gives a prescription for producing a Kagomé lattice.)

The single-particle states of atoms in an optical lattice potential, like those of electrons in a crystal, can be divided into bands, with each state assigned a crystal momentum by Bloch's theorem. At the low temperatures achievable in experiments, only the lowest band is populated, and it is more convenient to choose a basis for the states within this band that is maximally localized in position space. There is then one such Wannier state [52, 53] for each minimum of the periodic potential.

An effective Hamiltonian can then be written in this basis, and a simple and important example is the Hubbard model [54], originally used to describe electrons

in a solid. In the case of spinless bosons [19, 48], it is often referred to as the Bose-Hubbard model and the Hamiltonian can be written

$$\mathcal{H} = -t \sum_{\langle ij \rangle} a_i^\dagger a_j + \frac{U}{2} \sum_i n_i(n_i - 1) \; . \tag{1.2}$$

Here, a_i is the annihilation operator for a boson in the Wannier state localized at site i of the lattice, and $n_i = a_i^\dagger a_i$ is the corresponding number operator. The first term allows for tunneling ('hopping') between adjacent sites: the notation $\langle ij \rangle$ denotes a sum over nearest-neighbor pairs of sites. The second term represents the mutual interaction of the atoms, and has been written to give a potential-energy 'cost' of U for every pair of atoms on the same site.[3]

The phase structure of the Bose-Hubbard model can be understood by considering separately the two limits $t/U \to 0$ and $t/U \to \infty$ [55, 56]. We assume that there is a fixed total number of atoms and that this is chosen so that the average number of atoms per site is an integer.

For $t = 0$, the model consists of a set of unconnected sites and the atoms will arrange themselves uniformly throughout the lattice, in order to minimize their mutual repulsion and hence the potential energy. This leads to an incompressible state, referred to as a Mott insulator. For a small nonzero t, virtual tunneling events will lead to fluctuations in the number on each site, but the system remains an incompressible insulator for a finite range of t/U.

In the opposite limit, where $U = 0$, there are no interactions between the particles and the bosons will condense into the single-particle state with the lowest energy. The system becomes a superfluid and remains so in the presence of a small finite U, but for sufficiently large U/t undergoes a transition into a Mott insulator. A simple

[3]Note that this simplification, which involves ignoring three-body and higher terms, is not necessary for the qualitative analysis, or the mean-field theory described below.

mean-field analysis was used in Ref. [55] to connect the two extremes and map out the phase diagram.

The superfluid–insulator phase transition was first demonstrated using cold atomic gases in the work of Greiner *et al.* [49], which used rubidium-87 atoms in an optical lattice. Superfluidity of (pairs of) fermions in an optical lattice has also been reported in Ref. [57].

1.3 Atoms with spin

Another common feature of condensed-matter systems, and one that leads to a great deal of interesting phenomena, is the presence of spin. While most of the species used in experiments with ultracold atoms have several hyperfine (nuclear spin) states, it required the development of purely optical trapping techniques [58] to liberate this degree of freedom.

For bosonic atoms, where the ground state (in the absence of a lattice) is a BEC, the condensate wavefunction has the possibility for interesting structure in spin space [59, 60], with the number of possible phases increasing with the atomic spin [61]. The actual ground state that is realized depends on the scattering lengths in the channels with different total spin.

The collective modes above each of these ground states and the response to an applied magnetic field can be determined using a semiclassical analysis of the dynamics of the condensate wavefunction. Also of interest is the dynamics of these systems when driven far from equilibrium. An example is the so-called 'spin-mixing' dynamics [62, 63], which describes the evolution of the occupation numbers of the different spin components when the system is initially far from its ground state.

In the presence of an optical lattice potential, there are, besides these condensed

phases, various possible insulating phases with different types of spin order [64–68]. The phase diagram is particularly rich when the filling factor (the ratio of the number of bosons to the number of sites in the lattice) is an even integer, in which case both superfluids and insulators, with and without spin ordering, are possible. Chapter 3 will consider this case and focus on the transition from an insulator to a superfluid in the absence of spin ordering.

1.4 Outline

This thesis is divided into two main parts, which address two examples of systems that may be realized using ultracold atomic gases.

Chapter 2: Bose-Fermi mixtures

This chapter is based on Ref. [69]. It is concerned with a mixture of bosonic and fermionic atoms coupled by a Feshbach resonance to a molecular state. The various phases of the mixture, assuming simultaneous degeneracy of all three species, are described. By varying the detuning, temperature and relative numbers of bosons and fermions, several different phases are found to be possible. We show that, at zero temperature, the phases can be distinguished by distinct Luttinger constraints that depend on the presence or absence of a Bose-Einstein condensate and also on the number of Fermi surfaces.

Chapter 3: Bosons with spin

This chapter, based in part on Ref. [70], describes a system of bosons with spin that are trapped within an optical lattice. We describe a mean-field theory that allows for the possibility of a paired condensate that does not break spin symmetry. We consider

the behavior of the Green function corresponding to single-particle excitations in the insulator and the paired superfluid and then show that, at the transition between the two, the coherent quasiparticles are replaced by an incoherent continuum with a nontrivial scaling exponent.

Chapter 4: Summary

This chapter summarizes the main results of this thesis and describes related ongoing and potential future work.

Chapter 2

Bose-Fermi mixtures

2.1 Introduction

In this chapter, we will consider a mixture of bosonic and fermionic atoms with a Feshbach resonance coupling the pair to a molecular state. Such a system is analogous those described in Section 1.1, with Feshbach resonances between a pair of fermions [30, 34–36] and a pair of bosons [37, 38].

In this case, the Feshbach resonance is a bound molecular state consisting of one bosonic and one fermionic atom, and hence is itself a fermion. The energy of the resonance can be tuned using an applied magnetic field, as described in Section 1.1, and the energy difference between the bound state and the lower end of the two-atom continuum will be referred to as the detuning ν.

Our primary result is that the mixture displays a variety of phases, distinguished by the number of Fermi surfaces and the presence or absence of a Bose-Einstein condensate (BEC). We will use mean-field theory to map out the phase diagram in terms of ν, the temperature T, and the densities of the two types of atom (see Figs. 2.1, 2.2, 2.3 and 2.6).

The existence of a quantum phase transition at zero temperature can be easily understood by considering the two limiting cases. For $\nu \gg 0$, molecules are strongly disfavored, leaving a BEC of the bosonic atoms and a Fermi surface of the fermionic atoms. In contrast, for $\nu \ll 0$, a Fermi surface of molecules will be formed. If the number of fermionic (N_f) and bosonic (N_b) atoms are unequal, there will also be some residual atoms which are not in molecules, and these form their own ground state. For $N_f > N_b$, the extra fermions will form a separate Fermi surface of atoms, while for $N_b > N_f$, the extra bosons will form an atomic BEC.

Note that for $N_f > N_b$, changing the detuning takes the system between limits with and without an atomic BEC. There must therefore be a critical detuning at which the atomic BEC is completely depleted, and all the bosonic atoms have been absorbed into molecules.

The number of Fermi surfaces also changes as the detuning is varied, and we will show in Section 2.5 that the statement of Luttinger's theorem is different in each phase. In the absence of a BEC, there are generically two Fermi surfaces, one atomic and one molecular, and their volumes are separately constrained. In the presence of a BEC, there may be either one or two Fermi surfaces, but there is only a single Luttinger constraint. In the phase with two Fermi surfaces and a BEC, the *total* volume of the Fermi surfaces is fixed by the number of fermionic atoms.

We now give an outline of the contents of the rest of this chapter. First, in Section 2.2, we define the model Hamiltonian that will be used throughout. In Section 2.3, we consider the limit of vanishing coupling, which was also described by the earlier work of Yabu *et al.* [71]. In this limit, the properties of the mixture are described by purely thermodynamic considerations and these can be used to map out the phase diagram.

Section 2.4 finds the phase structure for finite coupling, treating quantum effects

using a mean-field approach. In Section 2.5, we describe our results regarding Luttinger's theorem for the system. In Section 2.6, the mean-field result of Section 2.4 is reproduced using a field-theoretical approach, which further allows us to characterize the critical properties of the transition.

In Section 2.7, we estimate the corrections to, and region of validity of, mean-field theory. Finally, in the appendix, we address the physics of an isolated molecule, and then consider the stability of the system against separation into two regions with different densities.

2.2 Basic definitions

The system consists of bosonic atoms b and fermionic atoms f which combine to form fermionic molecules ψ. The energy, relative to the chemical potential μ, is for the atoms

$$\xi_{\mathbf{k}}^{f} = \epsilon_{\mathbf{k}}^{f} - \mu^{f} = \frac{k^2}{2m^{f}} - \mu^{f} \tag{2.1}$$

$$\xi_{\mathbf{k}}^{b} = \epsilon_{\mathbf{k}}^{b} - \mu^{b} = \frac{k^2}{2m^{b}} - \mu^{b} \tag{2.2}$$

and for the molecule

$$\xi_{\mathbf{k}}^{\psi} = \epsilon_{\mathbf{k}}^{\psi} - \mu^{\psi} = \frac{k^2}{2m^{\psi}} - \mu^{\psi} + \nu \ , \tag{2.3}$$

including the detuning ν. The masses obey $m^{\psi} = m^{f} + m^{b}$ and, because of the interaction, the chemical potentials are related by $\mu^{\psi} = \mu^{f} + \mu^{b}$.

The grand-canonical Hamiltonian is, in momentum space,

$$\mathcal{H} = \int \frac{\mathrm{d}^3\mathbf{k}}{(2\pi)^3} \left(\xi_{\mathbf{k}}^{f} f_{\mathbf{k}}^{\dagger} f_{\mathbf{k}} + \xi_{\mathbf{k}}^{b} b_{\mathbf{k}}^{\dagger} b_{\mathbf{k}} + \xi_{\mathbf{k}}^{\psi} \psi_{\mathbf{k}}^{\dagger} \psi_{\mathbf{k}}\right) + \mathcal{H}_{\mathrm{int}} \ , \tag{2.4}$$

where $f_{\mathbf{k}}$, $b_{\mathbf{k}}$ and $\psi_{\mathbf{k}}$ are annihilation operators for the three species, at momentum $\mathbf{k}$.

We assume that the fermions' spins are polarized along the direction of the applied magnetic field, so that both f and ψ can be treated as spinless. The interaction term $\mathcal{H}_{\rm int}$ is given by

$$\mathcal{H}_{\rm int} = -\,g \int_{\mathbf{k},\mathbf{k}'} (\psi^\dagger_{\mathbf{k}+\mathbf{k}'} f_{\mathbf{k}} b_{\mathbf{k}'} + b^\dagger_{\mathbf{k}'} f^\dagger_{\mathbf{k}} \psi_{\mathbf{k}+\mathbf{k}'}) + \lambda \int_{\mathbf{k},\mathbf{k}',\mathbf{k}'} b^\dagger_{\mathbf{k}+\mathbf{k}'} b^\dagger_{\mathbf{k}'-\mathbf{k}'} b_{\mathbf{k}'}\, b_{\mathbf{k}}\ , \tag{2.5}$$

where $\int_{\mathbf{k}}$ denotes $\int \mathrm{d}^3\mathbf{k}\,/(2\pi)^3$. (We will consider the case of three spatial dimensions throughout, but the results can be generalized straightforwardly.)

The first term in $\mathcal{H}_{\rm int}$ allows the bosonic and fermionic atoms to couple and form molecules, while the second is an interaction between pairs of bosons. We omit quartic interactions for the fermions because the exclusion principle forbids s-wave scattering between identical fermions, and we assume that the other allowed interactions will be less important than the coupling g near resonance.

Taking the dimensions of momentum and energy to be unity, $[k] = [E] = 1$, we have $[\psi] = -\frac{3}{2}$ and the same for the operators b and f. (Throughout, we shall measure temperature, energy and frequency in the same units, so that $\hbar = k_{\rm B} = 1$.) The coupling constants have dimensions $[g] = -\frac{1}{2}$ and $[\lambda] = -2$.

At temperature $T = 1/\beta \neq 0$, we have six dimensionless parameters. First let N_b be the total density of bosonic atoms, including those bound in molecules, and let N_f be the same for fermionic atoms. (We consider a unit volume, so that density is synonymous with number.) In the absence of any fermions, the bosons would condense at a temperature [5, 6]

$$T_0 = \frac{2\pi}{m^b}\left[\frac{N_b}{\zeta(\frac{3}{2})}\right]^{\frac{2}{3}}\ . \tag{2.6}$$

We can take as dimensionless parameters $T/T_0 = \beta_0/\beta$, N_f/N_b, m^f/m^b, ν/T_0, γ^2/T_0

and $\lambda^2 (m^b)^3 T_0$, where

$$\gamma = \frac{g^2}{8\pi} \left(\frac{2 m^f m^b}{m^\psi} \right)^{3/2} . \tag{2.7}$$

In what follows, it will not usually be necessary to take account of the coupling between bosons given by the final term of $\mathcal{H}_{\rm int}$. Except within the condensed phase, the main effect of λ is a renormalization of the boson mass, which can be incorporated into a redefinition of m^b.

Physical units

In order to relate these parameters to experimental values, we may choose a unit of volume of $10^{-15}\,\mathrm{cm}^3$, which gives the unit of momentum as roughly $10^{-27}\,\mathrm{kg \cdot m/s}$. Taking the unit of mass to be 6 amu, corresponding to a lithium-6 atom, the unit of energy is roughly $7 \times 10^{-10}\,\mathrm{eV}$ or $8\,\mu\mathrm{K}$.

To estimate the parameters of the Feshbach resonance, we use the expression [24]

$$g = \sqrt{\frac{2\pi a_{\rm bg}\, \Delta B \Delta\mu}{m}} , \tag{2.8}$$

where $a_{\rm bg}$ is the background scattering length, ΔB is the width of the resonance and $\Delta\mu$ is the difference in magnetic moments. Using the observed background scattering length between lithium-6 and -7 of $a_{\rm bg} = 2.0\,\mathrm{nm}$ [43], we may estimate the coupling constant. Taking, for instance $\Delta B = 1\,\mathrm{G}$, $\Delta\mu = \mu_{\rm B}$, the Bohr magneton, we find $g \simeq 1$ in our units. For a boson density $N_b = 10^{15}\,\mathrm{cm}^{-3}$ and mass $m^b = m^f = 6\,\mathrm{amu}$, the value $g = 1$ gives a dimensionless coupling of $\gamma^2/T_0 = 5 \times 10^{-4}$.

While the width of the resonance used here, $\Delta B = 1\,\mathrm{G}$, is sufficiently large that $\Delta\mu\Delta B \gtrsim T_0$, it is nonetheless somewhat smaller than typical experimental values. For our purposes, a more relevant measure of the resonance 'width' is the lifetime of the molecule state in the vacuum (for $\nu > 0$). This is calculated in Section A.1

of the appendix, where we show that it is determined by the constant γ. Since the relevant energies are on the order of T_0, the condition for a narrow resonance is that $\gamma^2/T_0 \ll 1$. For the numerical results throughout this paper, we will always remain in this narrow limit, which is analytically more accessible. As noted above, we expect our results to be at least qualitatively applicable even for the wider Feshbach resonances observed experimentally.

Following Ref. [38], we take

$$\lambda = \frac{2\pi}{m^b} a_{bb} \,, \tag{2.9}$$

where for a_{bb}, the scattering length for the boson–boson interaction, we use $a_{bb} = 0.27\,\mathrm{nm}$ [43], giving

$$\lambda^2 (m^b)^3 T_0 = 2 \times 10^{-3} \,. \tag{2.10}$$

The detuning ν appearing in the molecular dispersion relation, Eq. (2.3), is given by [24]

$$\nu = \Delta\mu (B - B_0) \,, \tag{2.11}$$

where B_0 is the magnetic field at resonance and B is the applied field.

2.3 The limit $g \to 0$

The case of vanishing coupling, which can be addressed with a classical approach, has been considered by Yabu *et al.* [71]. (The results presented in this section produce Fig. 3 of Ref. [71], which corresponds to our Fig. 2.3, below.)

For simplicity, we restrict the analysis to zero temperature, but similar arguments can be made for nonzero temperatures. We call the two Fermi energies ϵ_0^f and ϵ_0^ψ, and the corresponding wavenumbers k_0^f and k_0^ψ. At zero temperature, all bosons are at $\epsilon^b = 0$ and fermionic atoms or molecules must be added at their respective Fermi

levels.[1]

The atomic Fermi surface (FS) vanishes when all the fermionic atoms are contained in molecules, so that

$$k_0^{\psi} = (6\pi^2 N_f)^{1/3} . \tag{2.12}$$

(The number of states within a unit sphere in momentum space is $1/6\pi^2$.) For this arrangement to be favorable energetically, the molecular Fermi energy, ϵ_0^{ψ}, must remain below the lowest atomic energy level. The boundary of the phase without an atomic FS is therefore where

$$\frac{1}{2m^{\psi}}(N_f)^{2/3} + \frac{\nu}{(6\pi^2)^{2/3}} = 0 . \tag{2.13}$$

Similarly, the molecular FS vanishes at the point when

$$\frac{1}{2m^{f}}(N_f)^{2/3} - \frac{\nu}{(6\pi^2)^{2/3}} = 0 . \tag{2.14}$$

The atomic (molecular) FS is therefore only absent for negative (positive) detuning ν.

To find the boundary of the phase with a BEC, we must consider the depletion of the condensate. Bosons will take fermions and form molecules as long as their final energy is lower, ie $\epsilon_0^{\psi} < \epsilon_0^{f} + 0$. The phase boundary is therefore where $\epsilon_0^{f} = \epsilon_0^{\psi}$, which gives

$$\frac{1}{2m^{f}}(N_f - N_b)^{2/3} - \frac{1}{2m^{\psi}}(N_b)^{2/3} = \frac{\nu}{(6\pi^2)^{2/3}} , \tag{2.15}$$

where the wavenumbers have been determined from N_b and N_f, using the fact that

[1] Here and throughout this chapter, we make the important assumption that there is no 'Pauli blocking' between fermionic atoms and molecules. This implies, for instance, that a fermionic atom and a molecule can simultaneously occupy states with the same momentum. The assumption is justified provided that the molecule is sufficiently tightly bound that its wavefunction has negligible overlap with the low-momentum atomic plane-wave states of interest.

there is no condensate.

The resulting phase diagrams are shown as the dashed lines in Figs. 2.1 and 2.3, below. It should be noted that, in this limit, the coupling to fermionic atoms reduces the tendency of the bosons to condense. (The same is true at nonzero temperature.)

2.4 Mean-field theory

It is possible to go beyond the classical analysis used for vanishing coupling, by using mean-field theory. We will present here two parallel developments, in this section and Section 2.6. The first is based on single-particle quantum mechanics, using the mixing between the fermionic dispersion relations caused by the presence of a BEC. The second uses a field-theoretic approach and considers perturbative corrections to the bosonic propagator. The former has the advantage of giving a somewhat clearer physical picture, while the latter leads naturally to higher-order corrections.

In the remainder of this section, we present the quantum-mechanical approach, starting from the Hamiltonian in Eq. (2.4). First, in Section 2.4.1, we make a mean-field approximation and diagonalize the new Hamiltonian. We then find the condition that a BEC should be energetically favorable, within this approximation. Since the Hamiltonian is defined in the grand canonical ensemble, we must then relate the chemical potentials to the particle numbers, in Section 2.4.2.

In Section 2.4.3, we restrict our attention to the case of zero temperature, where transitions occur between states with different numbers of Fermi surfaces. We identify the positions of these transitions and present the full phase diagram for $T = 0$.

2.4.1 Mean-field Hamiltonian

To derive a mean-field theory, we make the Bogoliubov approximation [72], replacing the boson field $b_{\mathbf{k}}$ in Eq. (2.4) by a real constant φ. The mean-field Hamiltonian is then

$$\mathcal{H}_{\mathrm{mf}} = \int \frac{\mathrm{d}^3\mathbf{k}}{(2\pi)^3} \left[\xi^f_{\mathbf{k}} f^\dagger_{\mathbf{k}} f_{\mathbf{k}} + \xi^\psi_{\mathbf{k}} \psi^\dagger_{\mathbf{k}} \psi_{\mathbf{k}} - g\varphi(\psi^\dagger_{\mathbf{k}} f_{\mathbf{k}} + f^\dagger_{\mathbf{k}} \psi_{\mathbf{k}})\right] - \mu^b \varphi^2 + \lambda\varphi^4 \,, \tag{2.16}$$

which can be diagonalized to

$$\mathcal{H}_{\mathrm{mf}} = \int \frac{\mathrm{d}^3\mathbf{k}}{(2\pi)^3} \left(\xi^F_{\mathbf{k}} F^\dagger_{\mathbf{k}} F_{\mathbf{k}} + \xi^\Psi_{\mathbf{k}} \Psi^\dagger_{\mathbf{k}} \Psi_{\mathbf{k}}\right) - \mu^b \varphi^2 + \lambda\varphi^4 \,. \tag{2.17}$$

The dispersion relations for the mixed fermions F, Ψ are

$$\xi^{F,\Psi}_{\mathbf{k}} = \frac{1}{2}\left(\xi^f_{\mathbf{k}} + \xi^\psi_{\mathbf{k}}\right) \pm \frac{1}{2}\sqrt{\left(\xi^f_{\mathbf{k}} - \xi^\psi_{\mathbf{k}}\right)^2 + 4g^2\varphi^2} \,, \tag{2.18}$$

with the choice that $\xi^F_{\mathbf{k}} \geq \xi^\Psi_{\mathbf{k}}$ for all $\mathbf{k}$.

Since mixing causes the dispersion relations to separate, the total energy of the fermions is lowered by nonzero φ. This quantum-mechanical effect, in contrast to the purely classical effect described in Section 2.3, therefore acts to favor condensation.

We must analyze the energetics to determine the point at which a condensate becomes favorable. The grand free energy Φ is minimized at temperature $1/\beta$ by a Fermi-Dirac distribution of each of the fermionic species F and Ψ. Ignoring the thermal distribution of bosons, which does not depend on φ, the total free energy is

$$\Phi(\varphi) = -\mu^b \varphi^2 + \lambda\varphi^4 + R^F(\varphi) + R^\Psi(\varphi) \,, \tag{2.19}$$

where

$$R^x(\varphi) = -\frac{1}{\beta}\int\frac{\mathrm{d}^3\mathbf{k}}{(2\pi)^3}\,\log\left(1+e^{-\beta\xi^x_{\mathbf{k}}}\right)\,. \tag{2.20}$$

The phase transition to a state with nonzero φ occurs when the quadratic coefficient changes sign, ie, when

$$\Delta \equiv \frac{1}{2}\frac{\mathrm{d}^2\Phi}{\mathrm{d}\varphi^2}\bigg|_{\varphi=0} = 0\,. \tag{2.21}$$

Specifically, for negative Δ, nonzero φ is energetically favored, causing the bosons to condense. Using Eqs. (2.18), (2.19), and (2.20), we find

$$\Delta = -\mu^b + g^2\int\frac{\mathrm{d}^3\mathbf{k}}{(2\pi)^3}\,\frac{n_{\mathrm{F}}(\xi^f_{\mathbf{k}}) - n_{\mathrm{F}}(\xi^\psi_{\mathbf{k}})}{\xi^f_{\mathbf{k}} - \xi^\psi_{\mathbf{k}}}\,, \tag{2.22}$$

where n_{F} is the Fermi-Dirac distribution function. The integral equation $\Delta = 0$ can be solved numerically.

2.4.2 Particle numbers

Since experiments are necessarily performed at fixed particle number, the expressions for the numbers in terms of the chemical potentials must be found. Particles of the species b, f and ψ are not independently conserved, so the relevant quantities are N_f and N_b, the total numbers of fermionic and bosonic atoms, respectively (including those contained in molecules).

Within our mean-field theory, we must consider the mixed fermionic species F and Ψ. Since each contains one atomic fermion, we have

$$N_f = \int\frac{\mathrm{d}^3\mathbf{k}}{(2\pi)^3}\,\left[n_{\mathrm{F}}(\xi^\Psi_{\mathbf{k}}) + n_{\mathrm{F}}(\xi^F_{\mathbf{k}})\right]\,. \tag{2.23}$$

The number of bosons is (with $n_{\rm B}$ the Bose-Einstein distribution function)

$$N_b = \varphi^2 + \int \frac{{\rm d}^3\mathbf{k}}{(2\pi)^3} \left[n_{\rm B}(\xi^b_{\mathbf{k}}) + n_{\rm F}(\xi^\Psi_{\mathbf{k}}) \cos^2\theta_{\mathbf{k}} + n_{\rm F}(\xi^F_{\mathbf{k}}) \sin^2\theta_{\mathbf{k}} \right] , \tag{2.24}$$

where the first term represents the condensate, the first term in the integrand is the thermal distribution of the bosons, and $\theta_{\mathbf{k}}$ is the mixing angle.[2]

When $\varphi = 0$, such as along the boundary to the phase without a BEC, the expression for the number of bosons simplifies to

$$N_b = \int \frac{{\rm d}^3\mathbf{k}}{(2\pi)^3} \left[n_{\rm B}(\xi^b_{\mathbf{k}}) + n_{\rm F}(\xi^\psi_{\mathbf{k}}) \right] . \tag{2.25}$$

To locate this phase boundary for fixed particle numbers, we must find the values of μ^f and μ^b which give the required numbers and also satisfy $\Delta = 0$. (Of course, a third parameter must be tuned to its critical value to satisfy these three conditions simultaneously.)

Results from such a procedure are displayed in Fig. 2.1, which shows the boundary for $N_f/N_b = 1.11$ as a function of the detuning ν and temperature $T = 1/\beta$. The masses of the atoms are equal, $m^f = m^b$, and the solid line has dimensionless coupling $\gamma^2/T_0 = 2.5 \times 10^{-4}$. For comparison, the case of vanishing coupling, treated in Section 2.3, is also shown, with a dashed line. Both curves tend to $T = T_0$, as in the case of free bosons, when $\nu \to \infty$ so that molecules cannot be formed.

In Fig. 2.2, the same phase boundary is shown on a graph of fermion number versus detuning, for three different temperature values. The solid line is at zero temperature, $T = 0$, while the two dashed lines have nonzero temperatures. The coupling is $\gamma^2/T_0 = 2.5 \times 10^{-4}$ and the masses are equal, $m^f = m^b$. As expected,

[2]Explicitly, $\theta_{\mathbf{k}}$ is the angle parametrizing the unitary transformation from the fermions f and ψ in Eq. (2.16) to the fermions F and Ψ in Eq. (2.17).

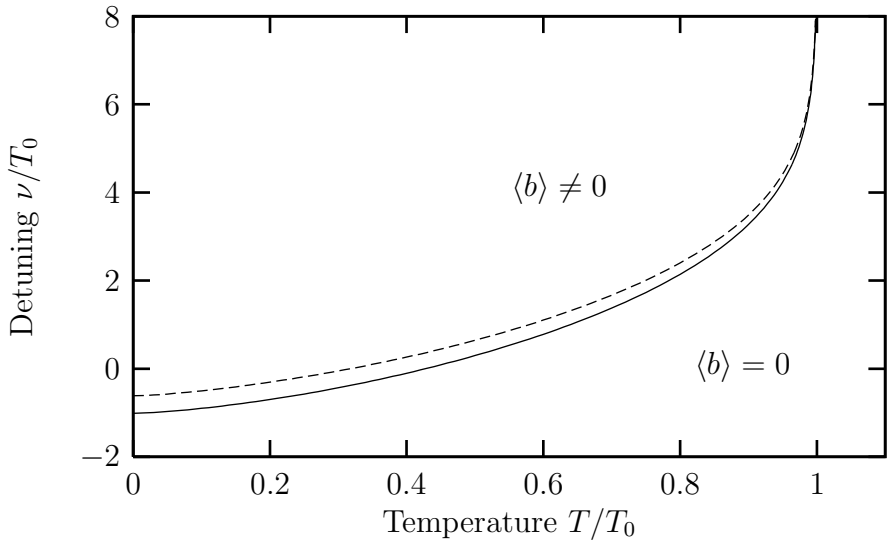

Figure 2.1: Phase boundary with detuning ν and temperature T, for fixed particle numbers $N_f/N_b = 1.11$ and equal atomic masses, $m^f = m^b$. The dashed line has vanishing coupling and has been found with a purely classical analysis. The solid line has dimensionless coupling $\gamma^2/T_0 = 2.0 \times 10^{-2}$, and has been determined using the mean-field theory of Section 2.4. For both, the condensed phase is on the left-hand side (for lower T) and labeled $\langle b\rangle \neq 0$, while the phase without a condensate is labeled $\langle b\rangle = 0$.

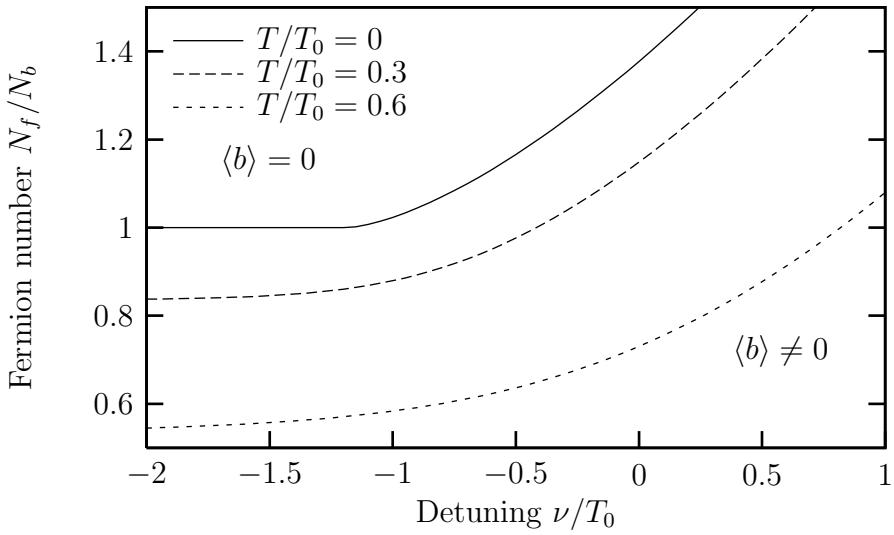

Figure 2.2: Phase boundary with fermion number N_f and detuning ν, for three different temperatures. The coupling is $\gamma^2/T_0 = 2.5 \times 10^{-4}$ and the atomic masses are equal. The two phases are labeled as in Fig. 2.1, with the condensed phase favored for higher detuning, lower fermion number and lower temperature.

Bose condensation is favored by lower temperatures, as in the case of an isolated Bose gas.

It remains to be shown that the system is stable against separation into regions with different densities. This question will be addressed in Section A.2 of the appendix.

2.4.3 Zero-temperature phases

At $T = 0$, the Fermi-Dirac distribution function is replaced by a unit step and all bosons occupy the lowest-energy state. As noted by Yabu *et al.* [71], the phase diagram can be further divided into a region with two Fermi surfaces and a region with a single Fermi surface. (We ignore the trivial case without any Fermi surfaces, which requires $N_f = 0$.)

Except when the atomic numbers precisely match, $N_f = N_b$, the case of a single

Fermi surface can only occur when there is a BEC. In this case, φ, the expectation value of b, is given by the minimum of the free energy Φ given in Eq. (2.19), so that we must solve

$$-2\mu^b\,\varphi + 4\lambda\,\varphi^3 + \frac{\mathrm{d}R^F}{\mathrm{d}\varphi} + \frac{\mathrm{d}R^\Psi}{\mathrm{d}\varphi} = 0 \tag{2.26}$$

(excluding the root $\varphi = 0$).

Following the choice that $\xi^F_{\mathbf{k}} \geq \xi^\Psi_{\mathbf{k}}$ in Eq. (2.18), the second Fermi surface disappears when $\xi^F_{\mathbf{k}=\mathbf{0}} = 0$, making the Fermi wavenumber for F fermions vanish. For this to be the case, we require $\mu^f > 0$, $\mu^\psi > \nu$ and

$$g\varphi = \sqrt{\mu^f(\mu^\psi - \nu)}\,, \tag{2.27}$$

which should be solved simultaneously with Eq. (2.26).

These expressions, along with the results in Section 2.4.2 for the particle numbers, allow the complete zero-temperature phase diagram to be plotted. In Fig. 2.3, the phase boundaries are shown on a graph of fermion number against detuning, for equal atomic masses. The three sets of boundaries have couplings (a) $\gamma^2/T_0 = 0$, (b) $\gamma^2/T_0 = 2.5\times10^{-4}$ and (c) $\gamma^2/T_0 = 2.0\times10^{-2}$. (Note that the dimensionless coupling γ^2/T_0 depends on the fourth power of the coupling g appearing in the Hamiltonian, so a large change in γ^2/T_0 is required for a noticeable change in the phase diagram. All of these coupling values are within the narrow resonance regime.) Throughout, we take $\lambda^2(m^b)^3T_0 = 2\times10^{-3}$; we have verified that, within a reasonable range of values, changing this parameter has no significant effect.

The boundaries divide the diagram into three regions, depending on the presence of a condensate and the number of Fermi surfaces. In the region labeled '2 FS, no BEC', the discriminant Δ is positive, so there is no BEC and two Fermi surfaces. In the region labeled '2 FS + BEC', Δ is negative and there is a condensate, as well

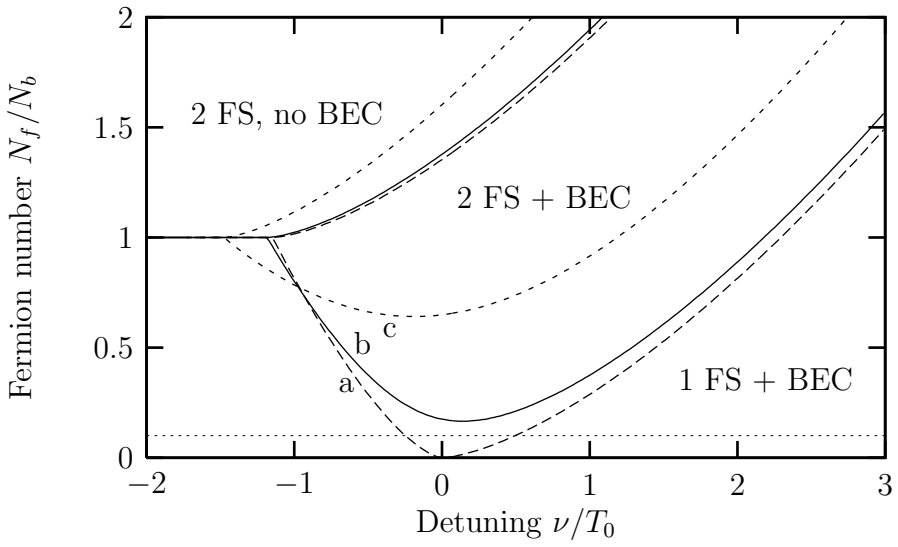

Figure 2.3: The phase diagram at $T = 0$ with dimensionless couplings (a) $\gamma^2/T_0 = 0$, (b) $\gamma^2/T_0 = 2.5 \times 10^{-4}$ and (c) $\gamma^2/T_0 = 2.0 \times 10^{-2}$. The atomic masses are equal and the coupling between bosons is given by $\lambda^2(m^b)^3 T_0 = 2 \times 10^{-3}$. The three distinct phases have, respectively, no Bose-Einstein condensate and two Fermi surfaces (labeled '2 FS, no BEC'), a condensate and two Fermi surfaces ('2 FS + BEC'), and a condensate and a single Fermi surface ('1 FS + BEC'). The dotted line indicates the fermion number at which Fig. 2.4 is plotted.

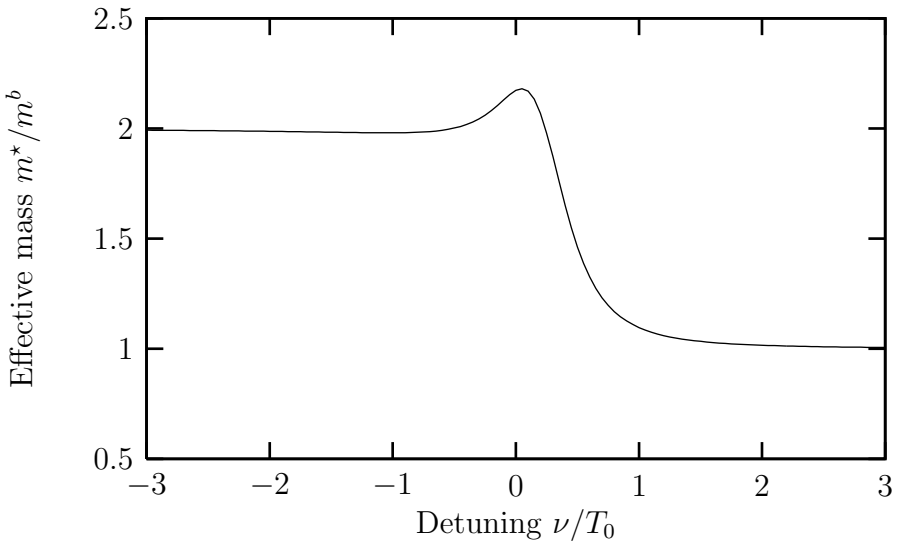

Figure 2.4: The effective mass $m^\star$ at the Fermi surface, with fermion number $N_f = 0.1N_b$, coupling $\gamma^2/T_0 = 2.5 \times 10^{-4}$, and equal atomic masses. As can be seen from the dotted line in Fig. 2.3, these parameters give a phase with a single Fermi surface. This surface changes from having a molecular character, with $m^\star \simeq m^\psi$, to having an atomic character, $m^\star \simeq m^f$.

as two Fermi surfaces. The lowermost region of the diagram, '1 FS + BEC', has a condensate and only a single Fermi surface.

For curve (a), with $\gamma^2/T_0 = 0$ (as in Section 2.3), the boundary between the regions with one and two Fermi surfaces extends down to $N_f = 0$. The region with a single Fermi surface is then divided into two, with the left-hand side having a Fermi surface of molecules and the right-hand side a Fermi surface of atoms. When $\gamma^2/T_0 \neq 0$, these two regions are no longer distinct, with the single Fermi surface crossing over from having a molecular character on one side (lower ν) to having an atomic character on the other (higher ν).

This crossover is illustrated in Fig. 2.4, where the effective mass $m^\star$ at the Fermi surface is plotted. The fermion number is set at $N_f = 0.1N_b$ and the coupling is $\gamma^2/T_0 = 2.5 \times 10^{-4}$, so that the system is within the phase with a single Fermi

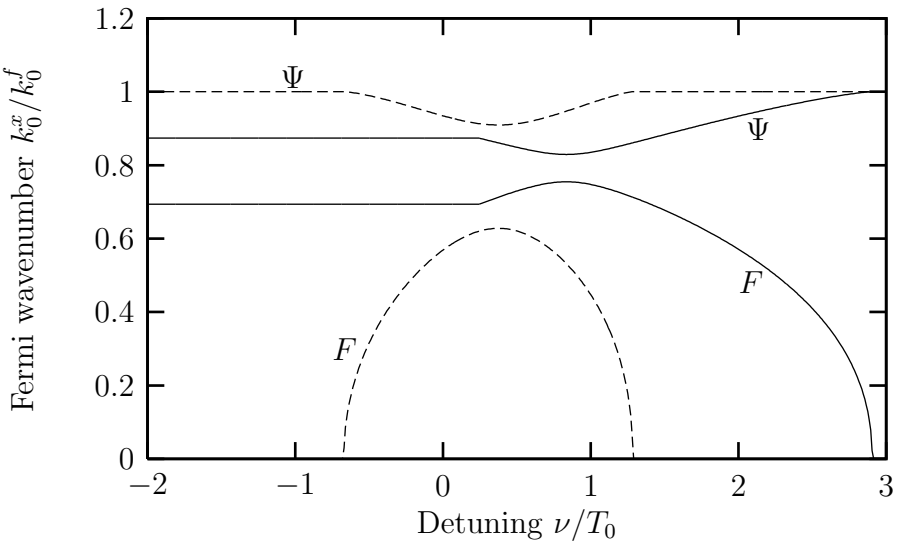

Figure 2.5: The Fermi wavenumbers for the two mixed species of fermions, Ψ and F, with coupling $\gamma^2/T_0 = 2.5 \times 10^{-4}$ and equal atomic masses. The solid lines have fermion number $N_f = \frac{3}{2}N_b$, while the dashed lines have $N_f = \frac{1}{2}N_b$. As can be seen in Fig. 2.3, the solid line goes between all three phases (at $\nu/T_0 \simeq 0.25$ and $\nu/T_0 \simeq 2.9$), while the dashed line goes from the phase with a single Fermi surface to that having two and back again (at $\nu/T_0 \simeq -0.65$ and $\nu/T_0 \simeq 1.3$). The wavenumbers are measured in units of k_0^f, the Fermi wavenumber for free fermions with number N_f.

surface (of Ψ fermions). The effective mass is defined as

$$m^\star = \left(\frac{\mathrm{d}^2 \xi_{\mathbf{k}}^\Psi}{\mathrm{d}k^2}\bigg|_{k_0^\Psi} \right)^{-1} . \tag{2.28}$$

For $\nu \ll 0$, the Fermi surface has an essentially molecular character and $m^\star \simeq m^\psi$, while for $\nu \gg 0$, it is atom-like, with $m^\star \simeq m^f$.

In Fig. 2.5, the Fermi wavenumbers of the two fermionic species are plotted, for coupling $\gamma^2/T_0 = 2.5 \times 10^{-4}$ and two different fermion numbers, $N_f = \frac{3}{2}N_b$ (solid lines) and $N_f = \frac{1}{2}N_b$ (dashed lines). In both the phase without a condensate (solid lines for $\nu/T_0 < 0.25$) and the phase with a single Fermi surface (solid lines for $\nu/T_0 > 2.9$, dashed lines for $\nu/T_0 < -0.65$ and $\nu/T_0 > 1.3$), the wavenumbers are constant, due to the fixed particle numbers. Only in the phase with two Fermi

surfaces and a BEC do the Fermi wavevectors change with detuning. (At the fermion number used in Fig. 2.4, the system stays in the phase with a single Fermi surface throughout and $k_0^\Psi = k_0^f$, $k_0^F = 0$ for all detunings.) In Section 2.5, we will show that the constraints on the Fermi wavenumbers are consequences of Luttinger's theorem, and are not an artifact of mean-field theory.

We now briefly address the line dividing the phases '2 FS, no BEC' and '1 FS + BEC' in Fig. 2.3. This boundary is horizontal and starts at the point where the three phases meet; in Section 2.5, we will prove that this is at exactly $N_b = N_f$. At this transition, two changes occur: both the second Fermi surface vanishes and the BEC appears, as the line is crossed from above. Physically, this results from the fact that molecules are highly energetically favored in this region, so that as many molecules as possible are formed, and the residual atoms form their ground state. For $N_f > N_b$, these atoms are fermionic and form a Fermi surface, while for $N_f < N_b$, they are bosonic and form a condensate. Precisely at $N_f = N_b$, there are no residual atoms, so that there is no condensate and only a molecular Fermi surface.

Figure 2.6 shows the same phase diagram as Fig. 2.3, but with the chemical potential for the fermionic atoms, μ^f, on the vertical axis; the number of fermionic atoms is allowed to vary. In the region where $\mu^f > 0$, the essential features are unchanged, with the same three phases as shown in Fig. 2.3. The boundary between the phases '2 FS, no BEC' and '1 FS + BEC', however, is seen to extend into an entire phase, labeled '1 FS, no BEC'. In this region, there is no condensate and μ^f is negative, so that there is only one Fermi surface, of molecules. This entire phase therefore has $N_f = N_b$ and collapses onto a single line in Fig. 2.3. This situation resembles that in the Mott insulator lobes in the phase diagram of the Bose-Hubbard model (see Sections 1.2 and 3.2): the density of particles is insensitive to a change in the chemical potential μ^f.

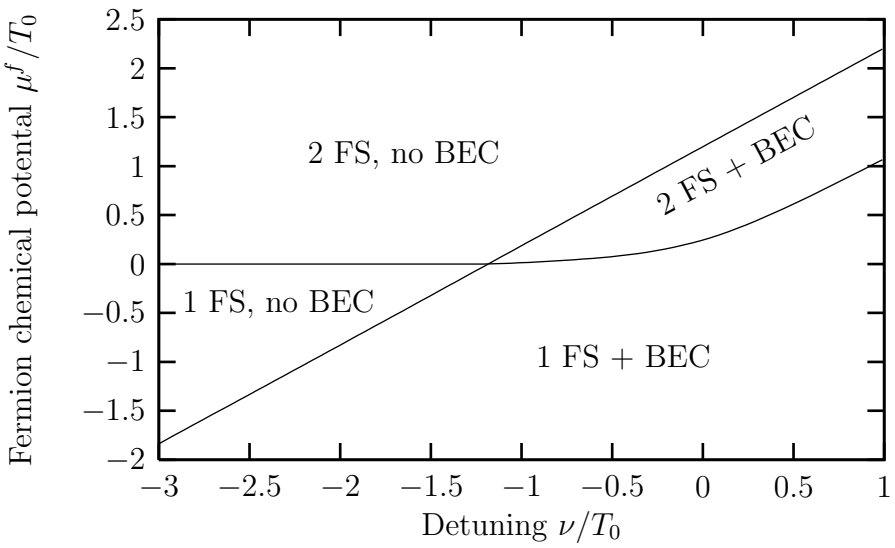

Figure 2.6: The phase diagram in the grand canonical ensemble, with the fermion chemical potential μ^f plotted on the vertical axis and the detuning ν on the horizontal axis. The number ratio N_f/N_b is allowed to vary in this plot. The boundary between '2 FS, no BEC' and '1 FS + BEC' in Fig. 2.3 expands into a new phase, labeled '1 FS, no BEC', within which there are only molecules, whose density is constant (both N_f and N_b remain fixed in this phase). The atomic masses are equal, and the couplings are $\gamma^2/T_0 = 2.5 \times 10^{-4}$ and $\lambda^2(m^b)^3 T_0 = 2 \times 10^{-3}$.

2.5 Luttinger's theorem

All the ground states in our phase diagram in Fig. 2.3 contain Fermi surfaces. In Fig. 2.5 we presented the evolution of the Fermi wavevectors of these Fermi surfaces in our mean-field calculation. In the present section we will discuss general constraints that must be satisfied by these Fermi wavevectors which are valid to all orders in the interactions. (Throughout this section, we shall be concerned only with $T = 0$.)

We will base our arguments upon the existence of the Luttinger-Ward functional [73] $\Phi_{\rm LW}$, satisfying

$$\Sigma = \left. \frac{\delta \Phi_{\rm LW}[G']}{\delta G'} \right|_{G'=G}, \tag{2.29}$$

where G' is a dummy variable, G is the actual full (thermal) Green function and Σ is the full self-energy. (Throughout this section, we will mostly be concerned with the full Green functions, which we shall denote with the symbol G. When we make reference to the free Green function, this will be denoted G_0.)

The Luttinger-Ward functional can be constructed nonperturbatively, starting from the partition function Z of the system [74]. It can then be shown straightforwardly that, treating the Green function as a matrix in its momentum (and frequency) indices, any unitary transformation of the free Green function, $G_0 \rightarrow UG_0U^{-1}$, that leaves Z invariant also leaves $\Phi_{\rm LW}$ invariant. A standard proof of Luttinger's theorem [75] for a system of interacting fermions makes use of the invariance of Z under a shift in the frequency appearing in the free propagator, $\omega \rightarrow \omega + \alpha$.

First, we consider the phase with no BEC. Here there are necessarily two Fermi surfaces, and, as we will now show, the volumes of the two Fermi surfaces are separately constrained, independently of the interactions.

In the present case, $\Phi_{\rm LW}$ is a functional of the three Green functions, one for each species, and Z is invariant under a simultaneous shift in two of the three frequencies,

ie,

$$\begin{aligned}\Phi_{\rm LW}[G^{\psi}(\mathrm{i}\nu_1), G^{f}(\mathrm{i}\nu_2), G^{b}(\mathrm{i}\omega)] \\ &= \Phi_{\rm LW}[G^{\psi}(\mathrm{i}\nu_1), G^{f}(\mathrm{i}\nu_2 - \mathrm{i}\alpha), G^{b}(\mathrm{i}\omega + \mathrm{i}\alpha)] \\ &= \Phi_{\rm LW}[G^{\psi}(\mathrm{i}\nu_1 + \mathrm{i}\beta), G^{f}(\mathrm{i}\nu_2), G^{b}(\mathrm{i}\omega + \mathrm{i}\beta)] \quad (2.30)\end{aligned}$$

for any α and β.

We now write $\mu^b = \mu^\psi - \mu^f$ and consider derivatives of the grand energy with respect to μ^f and μ^ψ. The derivative with respect to μ^f yields

$$\left\langle f^\dagger f \right\rangle - \left\langle b^\dagger b \right\rangle = N_f - N_b \; . \quad (2.31)$$

Each term on the left-hand side can be rewritten in terms of the full Green functions, giving

$$N_f - N_b = -\int \frac{\mathrm{d}^3\mathbf{k}\; \mathrm{d}\omega}{(2\pi)^4}\, \mathrm{e}^{\mathrm{i}\omega 0^+} \left[G^f_{\mathbf{k}}(\mathrm{i}\omega) + G^b_{\mathbf{k}}(\mathrm{i}\omega) \right] \; . \quad (2.32)$$

(The change of sign of the f term results from the anticommutation of fermion operators.)

From now on the manipulations are standard [75]. We make use of the identity

$$G(\mathrm{i}\omega) = \mathrm{i}G(\mathrm{i}\omega)\frac{\partial}{\partial\omega}\Sigma(\mathrm{i}\omega) - \frac{\partial}{\partial\omega}\log G(\mathrm{i}\omega) \; , \quad (2.33)$$

which results from the Dyson equation. The first equation of Eq. (2.30) gives, together with Eq. (2.29),

$$\int \frac{\mathrm{d}^3\mathbf{k}\; \mathrm{d}\omega}{(2\pi)^4} \left[\Sigma^b_{\mathbf{k}}(\mathrm{i}\omega)\frac{\partial}{\partial\omega} G^b_{\mathbf{k}}(\mathrm{i}\omega) + \Sigma^f_{\mathbf{k}}(\mathrm{i}\omega)\frac{\partial}{\partial\omega} G^f_{\mathbf{k}}(\mathrm{i}\omega) \right] = 0 \; . \quad (2.34)$$

Combining these two with Eq. (2.32) and integrating by parts gives

$$N_f - N_b = \mathrm{i} \int \frac{\mathrm{d}^3\mathbf{k}\ \mathrm{d}\omega}{(2\pi)^4}\, \mathrm{e}^{\mathrm{i}\omega 0^+} \frac{\partial}{\partial\omega} \Big[\log G^f_{\mathbf{k}}(\mathrm{i}\omega) + \log G^b_{\mathbf{k}}(\mathrm{i}\omega)\Big] \tag{2.35}$$

(with the boundary terms vanishing because $G(\mathrm{i}\omega) \sim 1/|\omega|$ for $|\omega| \to \infty$).

The integral over ω can be treated as a contour integration and closed above, due to the factor $e^{\mathrm{i}\omega 0^+}$. Changing the integration variable to $z = \mathrm{i}\omega$ replaces this by an integral surrounding the left half-plane. Since both of the full Green functions $G^{b,f}_{\mathbf{k}}(z)$ have all their nonanalyticities and zeroes on the line of real z, we can write this as

$$N_f - N_b = \mathrm{i} \int \frac{\mathrm{d}^3\mathbf{k}}{(2\pi)^3} \int_{-\infty}^{0} \frac{dz}{2\pi} \frac{\partial}{\partial z} \big[\log G^f_{\mathbf{k}}(z + \mathrm{i}0^+) + \log G^b_{\mathbf{k}}(z + \mathrm{i}0^+) - \log G^f_{\mathbf{k}}(z + \mathrm{i}0^-) - \log G^b_{\mathbf{k}}(z + \mathrm{i}0^-)\big] \ . \tag{2.36}$$

The integral of z can be performed trivially to give

$$N_f - N_b = \frac{\mathrm{i}}{2\pi} \int \frac{\mathrm{d}^3\mathbf{k}}{(2\pi)^3} \Big[\log G^f_{\mathbf{k}}(\mathrm{i}0^+) - \log G^f_{\mathbf{k}}(\mathrm{i}0^-) + \log G^b_{\mathbf{k}}(\mathrm{i}0^+) - \log G^b_{\mathbf{k}}(\mathrm{i}0^-)\Big] \ . \tag{2.37}$$

Using the analyticity properties of the Green functions, this can be written as

$$N_f - N_b = -\frac{1}{\pi} \int \frac{\mathrm{d}^3\mathbf{k}}{(2\pi)^3} \Big[\arg G^f_{\mathbf{k}}(\mathrm{i}0^+) + \arg G^b_{\mathbf{k}}(\mathrm{i}0^+)\Big] \ . \tag{2.38}$$

The reciprocals of the Green functions can now be written in terms of the free dispersions $\xi^{b,f}_{\mathbf{k}}$ and the exact self energies $\Sigma^{b,f}_{\mathbf{k}}$. The presence of well-defined quasiparticles in the low-energy limit implies that the imaginary part of the self energy must vanish for $\omega = 0$. The Green function is therefore real and its phase can be

written using the unit step function Θ, leaving

$$N_f - N_b = \int \frac{\mathrm{d}^3\mathbf{k}}{(2\pi)^3} \left[\Theta(-\xi^f_{\mathbf{k}} + \Sigma'^f_{\mathbf{k}}) + \Theta(-\xi^b_{\mathbf{k}} + \Sigma'^b_{\mathbf{k}})\right] , \tag{2.39}$$

where Σ' denotes the real part of the self energy evaluated for $\omega = 0$.

By definition, the absence of a BEC requires that there be no bosonic quasiparticle excitations at or below the chemical potential, so that the second term in the brackets in Eq. (2.39) vanishes. (Note that this does not imply that $\langle b^\dagger b \rangle = 0$, which is not the case beyond mean-field order.) This leaves the statement of Luttinger's theorem for this case:

$$N_f - N_b = \int \frac{\mathrm{d}^3\mathbf{k}}{(2\pi)^3} \Theta(-\xi^f_{\mathbf{k}} + \Sigma'^f_{\mathbf{k}}) . \tag{2.40}$$

The right-hand side of this expression is interpreted as the (reciprocal-space) volume of the atomic Fermi surface.

A similar result follows by taking the derivative of the grand energy with respect to μ^ψ, which gives

$$\langle \psi^\dagger \psi \rangle + \langle b^\dagger b \rangle = N_b . \tag{2.41}$$

Going through the same manipulations as above leads to

$$N_b = \int \frac{\mathrm{d}^3\mathbf{k}}{(2\pi)^3} \left[\Theta(-\xi^\psi_{\mathbf{k}} + \Sigma'^\psi_{\mathbf{k}}) - \Theta(-\xi^b_{\mathbf{k}} + \Sigma'^b_{\mathbf{k}})\right] , \tag{2.42}$$

corresponding to Eq. (2.39). In the phase with no BEC, this gives

$$N_b = \int \frac{\mathrm{d}^3\mathbf{k}}{(2\pi)^3} \Theta(-\xi^\psi_{\mathbf{k}} + \Sigma'^\psi_{\mathbf{k}}) . \tag{2.43}$$

We have therefore proved that there are two statements of Luttinger's theorem in the phase with two Fermi surfaces and no BEC. One, Eq. (2.40), states that

the volume of the atomic Fermi surface is fixed by the difference in the numbers of atomic fermions and bosons, while the other, Eq. (2.43), states that the volume of the molecular Fermi surface is fixed by the total number of bosonic atoms.

Similar considerations apply to the phases with a BEC, which may have either one or two Fermi surfaces. Here we show that Luttinger's theorem only demands that the total volume enclosed within *both* Fermi surfaces is determined by N_f; the volumes of the two Fermi surfaces (if present) are not constrained separately.

The same manipulations as above apply in the presence of a BEC, with two differences. Firstly, the species f and ψ can no longer be considered separately and instead, the Green functions for the hybridized species F and Ψ should be used. Secondly, it is no longer the case that the second term in the brackets vanishes in Eq. (2.39) and Eq. (2.42). Instead, if we add these two equations, we arrive at

$$N_f = \int \frac{\mathrm{d}^3\mathbf{k}}{(2\pi)^3}\,\Theta(-\xi^F_{\mathbf{k}} + \Sigma'^F_{\mathbf{k}}) + \int \frac{\mathrm{d}^3\mathbf{k}}{(2\pi)^3}\,\Theta(-\xi^\Psi_{\mathbf{k}} + \Sigma'^\Psi_{\mathbf{k}})\ . \tag{2.44}$$

The two terms in this expression give the volumes of the two Fermi surfaces. We see that their sum is constrained by the number of fermionic atoms.

Multicritical point

A simple application of our statements of Luttinger's theorem can be used to show that the multicritical point, where the three phases meet in Fig. 2.3 (and where four phases meet in Fig. 2.6), occurs at precisely $N_b = N_f$.

Firstly, according to Eq. (2.40), the volume of the atomic Fermi surface is given by $N_f - N_b$, as long as there is no BEC. This is therefore the case on the line dividing the phases with and without condensates, since the condensate vanishes as this line is approached from below. Secondly, the line that divides the regions with one and

two Fermi surfaces is the point where the atomic Fermi surface vanishes. Where the two lines meet, we see both that Eq. (2.40) is satisfied and that its right-hand side vanishes. We therefore have $N_b = N_f$.

2.6 Quantum phase transitions

We now present an alternative analysis using the language of field theory. In Section 2.6.1, we reproduce the result that Eq. (2.22) determines the presence of a condensate. Then, in Section 2.6.2, we determine the boson propagator near the BEC depletion transition. In Section 2.6.3, we describe the critical field theories for the various transitions.

For simplicity, we will restrict our attention here to the phase without a condensate; the extension to the condensed phases requires the standard Bogoliubov transformation to new degrees of freedom for the boson [5,6,11]. Even with this simplification, we will be able to consider the approach to the condensation transition from the uncondensed side, and derive the appropriate critical field theory.

The dimensionless Euclidean action corresponding to the Hamiltonian, Eq. (2.4), is

$$\mathcal{S} = \frac{1}{\beta}\sum_q \bar{f}_q \Xi^f_q f_q + \frac{1}{\beta}\sum_p \bar{b}_p \Xi^b_p b_p + \frac{1}{\beta}\sum_q \bar{\psi}_q \Xi^\psi_q \psi_q + \mathcal{S}_{\rm int} \ , \tag{2.45}$$

where

$$\mathcal{S}_{\rm int} = -\frac{g}{\beta^2}\sum_{p,q}\left(\bar{\psi}_q f_{q-p} b_p + \bar{b}_p \bar{f}_{q-p}\psi_p\right) \ . \tag{2.46}$$

The symbol p stands for $\mathbf{k}$ and ω_n, and likewise q for $\mathbf{k}'$ and ν_m, where the Matsubara frequencies ω_n (ν_m) are even (odd). The summations over p (q) represent sums over

ω_n (ν_m) and integrals over the momentum $\mathbf{k}$ ($\mathbf{k}'$). We have also defined

$$\Xi_p = (G_p)^{-1} = -\mathrm{i}\omega_n + \xi_{\mathbf{k}} \ , \tag{2.47}$$

the inverse of the free Green function, G_p, and similarly Ξ_q. (In this section and the following, we will use the symbol G to denote the free Green function, contrary to the notation of Section 2.5.)

We have omitted from the action the coupling term between pairs of bosons, since its effect is the same as in the standard analysis of the condensation transition [11,56], and we assume that this is less important than the near-resonance coupling to the fermions.

Integrating out both of the fermions and expanding the resulting coupling term to quadratic order in b and $\bar{b}$, we find that the effective action for the bosons is

$$\mathcal{S}^{(2)}_{\mathrm{eff}}[b,\bar{b}] = \frac{1}{\beta}\sum_p \bar{b}_p \Xi^b_p b_p + \frac{g^2}{\beta^2}\sum_{p,q} G^f_q G^\psi_{q+p} \bar{b}_p b_p \ . \tag{2.48}$$

2.6.1 Mean-field approximation

By replacing b by a real constant φ, we should arrive at the results of Section 2.4. In this approximation, we have

$$\mathcal{S}^{(2)}_{\mathrm{eff}}[b,\bar{b}] = -\mu^b \varphi^2 + \frac{g^2}{\beta}\varphi^2 \sum_q G^f_q G^\psi_q \ , \tag{2.49}$$

so that the coefficient is

$$\Delta = -\mu^b + g^2 \int \frac{\mathrm{d}^3\mathbf{k}'}{(2\pi)^3}\, \frac{1}{\beta}\sum_{\nu_m} G^f_{\mathbf{k}'}(\mathrm{i}\nu_m)\, G^\psi_{\mathbf{k}'}(\mathrm{i}\nu_m) \ . \tag{2.50}$$

The phase transition will occur when the coefficient Δ vanishes.

We can represent Eq. (2.50) by

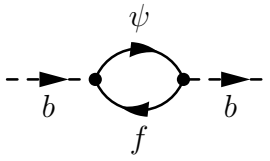

, (2.51)

which appears as a self-energy diagram in the boson propagator, drawn as a dashed line. (The two solid lines represent fermion propagators.)

The Matsubara sum can be performed by replacing it by a contour integration, giving

$$\Delta = -\mu^b + g^2 \int \frac{\mathrm{d}^3\mathbf{k}'}{(2\pi)^3} \, \frac{n_{\mathrm{F}}(\xi^f_{\mathbf{k}'}) - n_{\mathrm{F}}(\xi^\psi_{\mathbf{k}'})}{\xi^f_{\mathbf{k}'} - \xi^\psi_{\mathbf{k}'}} \, , \tag{2.52}$$

in agreement with Eq. (2.22).

2.6.2 Boson propagator

By retaining the frequency dependence of the boson field, but again keeping only terms quadratic in b and $\bar{b}$, we can determine the action for the long-wavelength, low-frequency excitations.

The effective boson propagator is, from Eq. (2.48), the reciprocal of

$$\begin{aligned} \widetilde{\Xi}^b_{\mathbf{k}}(\mathrm{i}\omega_n) &\equiv \Xi^b_p + \frac{g^2}{\beta} \sum_q G^f_q G^\psi_{q+p} \\ &= -\mathrm{i}\omega_n + \xi^b_{\mathbf{k}} + g^2 \int \frac{\mathrm{d}^3\mathbf{k}'}{(2\pi)^3} \, \frac{1}{\beta} \sum_{\nu_m} \frac{1}{-\mathrm{i}\nu_m + \xi^f_{\mathbf{k}'}} \frac{1}{-\mathrm{i}(\nu_m + \omega_n) + \xi^\psi_{\mathbf{k}'+\mathbf{k}}} \, , \end{aligned} \tag{2.53}$$

which replaces Eq. (2.50). For $\mathbf{k} = \mathbf{0}$, this gives

$$\widetilde{\Xi}^b_{\mathbf{0}}(\mathrm{i}\omega_n) = -\mathrm{i}\omega_n - \mu^b + g^2 \int \frac{\mathrm{d}^3\mathbf{k}'}{(2\pi)^3} \, \frac{n_{\mathrm{F}}(\xi^f_{\mathbf{k}'}) - n_{\mathrm{F}}(\xi^\psi_{\mathbf{k}'})}{\xi^f_{\mathbf{k}'} - \xi^\psi_{\mathbf{k}'} + \mathrm{i}\omega_n} \, , \tag{2.54}$$

where the result

$$n_{\rm F}(a - {\rm i}\omega_n) = n_{\rm F}(a) \ , \tag{2.55}$$

for ω_n a boson Matsubara frequency, has been used. For small ω_n, we can expand to give

$$\widetilde{\Xi}^b_{\mathbf{0}}({\rm i}\omega_n) \simeq \Delta - {\rm i}\omega_n \left[1 - g^2 \int \frac{{\rm d}^3\mathbf{k}'}{(2\pi)^3} \, \frac{n_{\rm F}(\xi^f_{\mathbf{k}'}) - n_{\rm F}(\xi^\psi_{\mathbf{k}'})}{\left(\xi^f_{\mathbf{k}'} - \xi^\psi_{\mathbf{k}'}\right)^2} \right] - \omega_n^2 g^2 \int \frac{{\rm d}^3\mathbf{k}'}{(2\pi)^3} \, \frac{n_{\rm F}(\xi^f_{\mathbf{k}'}) - n_{\rm F}(\xi^\psi_{\mathbf{k}'})}{\left(\xi^f_{\mathbf{k}'} - \xi^\psi_{\mathbf{k}'}\right)^3} \ . \tag{2.56}$$

(Note that, as required, the coefficient of ω_n^2 is in fact positive.)

The effective boson propagator (for $\mathbf{k} = \mathbf{0}$) is then

$$\widetilde{G}^b_{\mathbf{0}}({\rm i}\omega_n) = \frac{\mathcal{Z}}{-{\rm i}\omega_n + \tilde{\xi}^b_{\mathbf{0}}(\omega_n)} \ , \tag{2.57}$$

with

$$\mathcal{Z} = \left[1 - g^2 \int \frac{{\rm d}^3\mathbf{k}'}{(2\pi)^3} \, \frac{n_{\rm F}(\xi^f_{\mathbf{k}'}) - n_{\rm F}(\xi^\psi_{\mathbf{k}'})}{\left(\xi^f_{\mathbf{k}'} - \xi^\psi_{\mathbf{k}'}\right)^2} \right]^{-1} \ , \tag{2.58}$$

and

$$\tilde{\xi}^b_{\mathbf{0}}(\omega_n) = \mathcal{Z} \left[\Delta - \omega_n^2 g^2 \int \frac{{\rm d}^3\mathbf{k}'}{(2\pi)^3} \, \frac{n_{\rm F}(\xi^f_{\mathbf{k}'}) - n_{\rm F}(\xi^\psi_{\mathbf{k}'})}{\left(\xi^f_{\mathbf{k}'} - \xi^\psi_{\mathbf{k}'}\right)^3} \right] \ . \tag{2.59}$$

At zero temperature, the integrals in the expressions for both $\mathcal{Z}$ and $\tilde{\xi}^b_{\mathbf{0}}(\omega_n)$ diverge when the two Fermi wavenumbers coincide, which happens if $N_f = 2N_b$. For any other parameters, the integrals are finite, and the effective propagator has the form Eq. (2.57). As we discuss in the following subsection, this distinction leads to different field theories for the BEC depletion quantum transition for these cases.

2.6.3 Critical field theories

We now briefly outline the critical field theories that govern each of the quantum phase transitions; more details can be found in Ref. [69].

The phase diagrams in Figs. 2.3 and 2.6 contain two types of transitions: those where a Fermi surface appears (such as between '1 FS + BEC' and '2 FS + BEC'), and those where a BEC appears (such as between '2 FS, no BEC' and '2 FS + BEC'). The former are described by the theory of a dilute, noninteracting Fermi gas [56].

The second case is related to the transition occurring for isolated bosons at zero density, described in Refs. [55, 56], and has upper critical dimension $d = 2$. The critical theory is described by the effective action for the boson after integrating out the fermion modes, as in Section 2.6.2.

As noted above, however, in the special case that $N_f = 2N_b$, the atomic and molecular Fermi surfaces exactly coincide. The boson therefore couples to gapless fermionic excitations at zero momentum, giving nonanalytic terms in the effective action. These are described by the Hertz-Millis theory [56, 76, 77], originally applied to the onset of ferromagnetism in a Fermi liquid.

2.7 Gaussian corrections

In this section, we will provide an estimate of the region of applicability of the mean-field theory described above. To do so, we will consider the two-loop correction to the grand free energy Φ, near the condensation transition. This will result in corrections to the expressions found in Section 2.4.2 relating the chemical potentials to the particle numbers [34, 35]. We will estimate the range of parameters for which these corrections become significant.

The term in the Hamiltonian, Eq. (2.4), that couples the boson and fermion

produces no two-loop correction to the boson self energy. While a correction term does arise from the quartic boson interaction, we again assume that this is small in the region of interest. As in Section 2.6, we will simplify the analysis by restricting to the phase without a condensate.

The only two-loop correction to the free energy Φ is given by the diagram

$\Delta\Phi \quad =$ 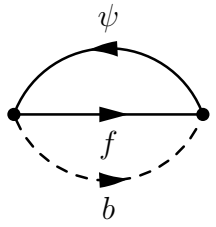

(2.60)

which represents the expression

$$\Delta\Phi = \frac{g^2}{\beta^2} \sum_{p,q} G^f_q G^\psi_{q+p} G^b_p \, . \tag{2.61}$$

Reinstating explicit momentum integrals and frequency sums, we have

$$\Delta\Phi = \frac{g^2}{\beta^2} \sum_{\omega_n,\nu_m} \int \frac{\mathrm{d}^3\mathbf{k}}{(2\pi)^3} \int \frac{\mathrm{d}^3\mathbf{k}'}{(2\pi)^3} \, G^b(\mathrm{i}\omega_n, \mathbf{k}) \, G^f(\mathrm{i}\nu_m, \mathbf{k}') \, G^\psi(\mathrm{i}\nu_m + \mathrm{i}\omega_n, \mathbf{k}' + \mathbf{k}) \tag{2.62}$$

Both Matsubara sums can be performed using contour integration, to give

$$\Delta\Phi = g^2 \int \frac{\mathrm{d}^3\mathbf{k}}{(2\pi)^3} \int \frac{\mathrm{d}^3\mathbf{k}'}{(2\pi)^3} \, \frac{\left[n_\mathrm{F}(\xi^f_{\mathbf{k}'-\mathbf{k}}) - n_\mathrm{F}(\xi^\psi_{\mathbf{k}'}) \right] \left[n_\mathrm{B}(\xi^b_{\mathbf{k}}) - n_\mathrm{B}(\xi^\psi_{\mathbf{k}'} - \xi^f_{\mathbf{k}'-\mathbf{k}}) \right]}{\xi^b_{\mathbf{k}} + \xi^f_{\mathbf{k}'-\mathbf{k}} - \xi^\psi_{\mathbf{k}'}} \, , \tag{2.63}$$

after a change of variables, $\mathbf{k}' \to \mathbf{k}' - \mathbf{k}$.

2.7.1 Renormalization of the detuning

As it stands, the integral over $\mathbf{k}$ is in fact divergent. As $k \equiv |\mathbf{k}|$ tends to infinity (with $|\mathbf{k}'|$ finite), the second Bose factor, $n_\mathrm{B}(\xi^\psi_{\mathbf{k}'} - \xi^f_{\mathbf{k}'-\mathbf{k}})$, tends to -1. In the first

bracket, $n_{\rm F}(\xi^{\psi}_{\mathbf{k}'})$ remains finite, so the integrand tends to $\sim 1/k^2$ and the integral over $\mathbf{k}$ is linearly divergent.

This divergence can be understood by considering the self-energy diagram

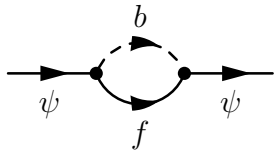

(2.64)

which gives a correction to the detuning ν linear in the cut-off momentum,

$$\nu = \nu_0 - g^2 \int \frac{{\rm d}^3\mathbf{k}}{(2\pi)^3} \, \frac{2m^f m^b}{m^{\psi}} \frac{1}{k^2} \; , \tag{2.65}$$

where ν_0 is the 'bare' detuning that appears explicitly in the action.

We use this expression to write ν_0, which appears within G^{ψ} in Eq. (2.61), in terms of ν, and then keep terms only of order g^2. The renormalized expression for $\Delta\Phi$ is then given by

$$\Delta\Phi = g^2 \int \frac{{\rm d}^3\mathbf{k}}{(2\pi)^3} \int \frac{{\rm d}^3\mathbf{k}'}{(2\pi)^3} \left\{ \frac{\left[n_{\rm F}(\xi^f_{\mathbf{k}'-\mathbf{k}}) - n_{\rm F}(\xi^{\psi}_{\mathbf{k}'}) \right] \left[n_{\rm B}(\xi^b_{\mathbf{k}}) - n_{\rm B}(\xi^{\psi}_{\mathbf{k}'} - \xi^f_{\mathbf{k}'-\mathbf{k}}) \right]}{\xi^b_{\mathbf{k}} + \xi^f_{\mathbf{k}'-\mathbf{k}} - \xi^{\psi}_{\mathbf{k}'}} + \frac{2m^f m^b}{m^{\psi}} \frac{n_{\rm F}(\xi^{\psi}_{\mathbf{k}'})}{k^2} \right\} , \tag{2.66}$$

where the dispersion relation ξ^{ψ} now involves the renormalized (physical) detuning ν. (We have retained the same symbols for the new, renormalized quantities.)

This expression can be simplified somewhat by performing a further change of variable, taking $\mathbf{k} \to \mathbf{k} + (m^b/m^{\psi})\mathbf{k}'$, and also making use of the result

$$n_{\rm B}(y-x)[n_{\rm F}(x) - n_{\rm F}(y)] = [1 - n_{\rm F}(x)]n_{\rm F}(y) \; . \tag{2.67}$$

We have finally

$$\Delta\Phi = g^2 \int \frac{\mathrm{d}^3\mathbf{k}}{(2\pi)^3} \int \frac{\mathrm{d}^3\mathbf{k}'}{(2\pi)^3} \frac{1}{\frac{m^\psi}{2m^f m^b}k^2 - \nu} \Bigg[n_{\mathrm{F}}(\xi^f) n_{\mathrm{B}}(\xi^b) - n_{\mathrm{F}}(\xi^\psi) n_{\mathrm{B}}(\xi^b) + n_{\mathrm{F}}(\xi^f) n_{\mathrm{F}}(\xi^\psi) - n_{\mathrm{F}}(\xi^\psi) \frac{2m^f m^b}{m^\psi} \frac{\nu}{k^2} \Bigg] , \quad (2.68)$$

in which the energies ξ^ψ, ξ^f and ξ^b should be evaluated at the following momenta:

$$\xi^\psi \equiv \xi^\psi(\mathbf{k}') \quad (2.69)$$

$$\xi^f \equiv \xi^f(\mathbf{k} - \tfrac{m^f}{m^\psi}\mathbf{k}') \quad (2.70)$$

$$\xi^b \equiv \xi^b(\mathbf{k} + \tfrac{m^b}{m^\psi}\mathbf{k}') \; . \quad (2.71)$$

Note that there is no singularity in the integral over $\mathbf{k}$ in Eq. (2.68), since the numerator also vanishes at the point where

$$k = \sqrt{\nu \frac{2m^f m^b}{m^\psi}} \quad (2.72)$$

(for $\nu > 0$).

2.7.2 Atom-number corrections

The expression for $\Delta\Phi$ must be differentiated with respect to the chemical potentials to give the correction to the number of each species of atom. The resulting integral can then be performed numerically.

The results of such a calculation are shown in Fig. 2.7, where we plot the corrections to the atom numbers, as a function of the dimensionless coupling γ^2/T_0. The number corrections have been divided by the total number of each atom evaluated to lowest order (as in Section 2.4.2). The detuning is held fixed at $\nu/T_0 = 0.5$ and

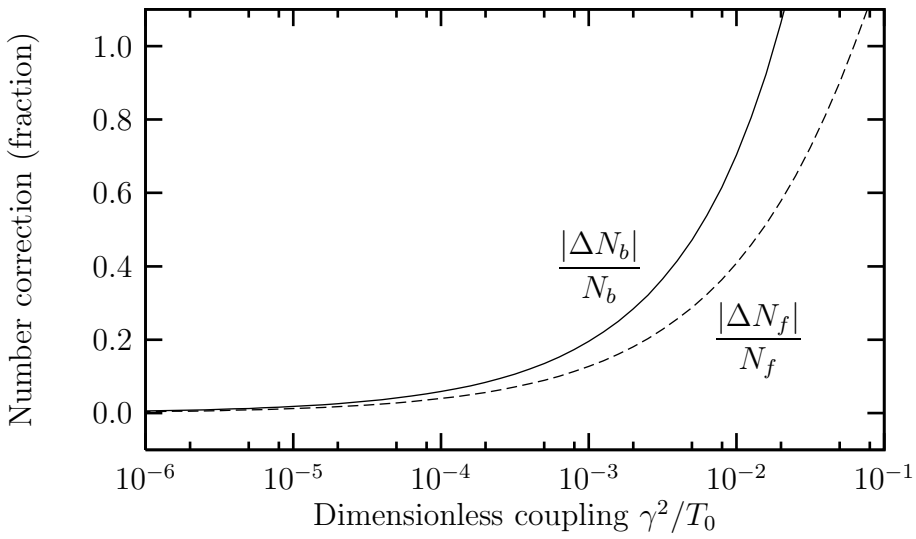

Figure 2.7: Two-loop corrections to the atom numbers, shown as a fraction of the total numbers evaluated to lowest order, and plotted as a function of the dimensionless coupling γ^2/T_0. The detuning is fixed at $\nu/T_0 = 0.5$, the atomic masses are equal, $m^f = m^b$, and the temperature is zero. At each value of the coupling, the parameters have been chosen to put the system just inside the '2 FS, no BEC' phase.

the atomic masses are equal; for simplicity, the temperature has been set to zero throughout. At every value of coupling, we have chosen the number ratio so that the system is in the phase '2 FS, no BEC' and close to the condensation transition.

The mean-field results can be expected to provide a quantitatively good approximation provided that the fractional corrections are small. Figure 2.7 suggests that this criterion is reasonably well satisfied for the coupling $\gamma^2/T_0 = 2.5 \times 10^{-4}$ used in Fig. 2.3. We expect only qualitative agreement at higher values of the coupling.

2.8 Conclusions

In this chapter, we have described the physics of a mixture of bosons and fermions that are able to form a bound molecular state. The resulting molecule is also a fermion and the mixture can form a variety of phases, distinguished by the number

of Fermi surfaces and the presence or absence of a Bose-Einstein condensate (BEC) of bosons.

The basic structure of the phase diagram can be determined by energetic considerations: The Pauli exclusion principle applies to both the atomic and molecular fermions and so the many-body ground state depends on the relative densities of both atomic species as well as the binding energy of the molecule. We extended this analysis using mean-field theory, showing that quantum-mechanical effects can favor the formation of a BEC and lead to 'mixing' of the atomic and molecular fermions.

We then showed that Luttinger's theorem, which constrains the volume of the Fermi surface(s), can be applied to these systems. The statement takes different forms depending on the presence or absence of a BEC. When a BEC is absent, the volumes of the molecular and atomic Fermi surfaces are separately constrained. When a BEC is present, only the sum of the two volumes is constrained.

The mean-field calculation can also be described in the language of quantum field theory, and this approach was used to investigate the critical properties at the various transitions. It was shown that the transition describing the appearance of the BEC is generically unaffected by the presence of the fermionic modes. In the special case that the two Fermi surfaces coincide, however, the gapless fermionic excitations give a critical theory of the Hertz-Millis form.

To determine the region of applicability of the mean-field calculation, we then found the two-loop corrections to the expressions for the atomic numbers. In Section A.1 of the appendix, we consider the dressed molecular propagator, and in Section A.2, we address the stability of the system to phase separation. In Chapter 4, some recent experiments on Bose-Fermi mixtures and possible extensions to the theory are described.

Chapter 3

Bosons with spin

3.1 Introduction

This chapter will describe the physics of bosonic atoms with spin, confined within an optical lattice. As described in Section 1.3, the simultaneous possibilities of spin and phase ordering lead to a very rich phase diagram. Our main focus will be the spin-singlet condensate (SSC), a condensed phase without spin ordering that occurs for bosons of any nonzero spin, provided that the spin-dependent interactions are strong enough.

When individual spinful bosons condense, spin-rotation invariance is necessarily broken, but when this is energetically unfavorable, singlet pairs will instead condense. For most atomic species, the spin-dependent part of the interaction is relatively weak, but an optical Feshbach resonance, described in Section 1.1, may be used to tune its strength.

From a theoretical point of view, the SSC phase is of particular interest because it provides a simple example of a condensate of pairs of bosons. (For similar examples that have been considered recently, see Refs. [37,38,78,79].) Such paired condensates

also provide an interesting analogue to the BCS phenomenon in superconductors, where singlet pairs of electrons form a superfluid [80].

Our primary interest will be the behavior of the system as this phase is approached across the quantum phase transition from the neighboring insulator (spin-singlet insulator, SSI). This transition corresponds to the appearance of a condensate of pairs, as the gap to 'doubly-charged' spin-singlet pair excitations vanishes, but the gap to 'singly-charged' excitations remains nonzero. (Here and throughout, we use the term 'charged' to refer to excitations that change the particle number, assigning to particles and holes charges of $+1$ and -1 respectively. This is simply for convenience: the bosons have no electric charge and feel no long-range forces.)

This leads to nontrivial long-time—or, equivalently, low-frequency—behavior of the Green function for spin-carrying excitations. Consider first the single-particle Green function for the elementary bosons. We will argue below that, near the critical point, the dispersion of this gapped excitation is an irrelevant perturbation, and so to leading order the analysis becomes a quantum *impurity* problem. A similar conclusion was reached in Refs. [81, 82] for the case of gapped fermionic excitations in a different context.

If the coupling between the localized (single particle) and bulk (pair) excitations is relevant, then a renormalization group (RG) analysis is necessary to understand the structure of the Green function. We will present such an analysis here, and show that a nontrivial impurity fixed point controls the long-time physics. For the case of an irrelevant localized–bulk coupling, no new impurity dimensions are needed, and the bulk fixed point governs the physics.

Similar results also apply for the correlation functions of composite operators, such as the spin-response function. We will show that these operators can be classified by their symmetry properties and that different anomalous dimensions apply in each

case.

We now give an outline of the contents of the rest of this chapter. We will begin in Section 3.2 with a presentation of the model Hamiltonian and a simple description of its phases. We will then describe the continuum theory of the model, which will be used to analyze the behavior across the phase transition to the SSC phase.

In Section 3.3, we describe a simple mean-field theory that explicitly incorporates the possibility of the SSC phase, and show that it occurs only when the spin-dependent part of the interaction is strong enough to overcome the kinetic-energy cost associated with condensing pairs of bosons.

In Section 3.4, we will describe the behavior of the single-particle Green function on both sides of the SSI–SSC transition. Then, in Section 3.5, we will address the transition itself and present the RG calculation that allows the scaling dimensions to be found. We will perform the analysis using dimensional regularization, which leads to the simplest explicit calculations. In Section A.3 of the appendix, we present an alternative derivation using a momentum cutoff, in which the physical interpretation is clearer.

3.2 Model

3.2.1 Hamiltonian

The application of the Bose-Hubbard model to bosonic atoms trapped in an optical lattice potential has been described above, in Section 1.2. The extension of this model to the case where the bosons carry spin is straightforward. While most of our results apply for general spin $F \neq 0$, we will treat explicitly the case $F = 1$ and draw attention to the generalizations when appropriate. The Hamiltonian can then

be written as

$$\mathcal{H} = -t \sum_{\langle i,j \rangle} (b^\dagger_{i\mu} b_{j\mu} + \text{h.c.}) + \sum_i V(b^\dagger_{i\mu} b_{i\mu}) + J \sum_i |\mathbf{L}_i|^2 \ , \tag{3.1}$$

where summation over repeated spin indices μ is implied throughout. The operator $b_{i\mu}$ annihilates a boson at site i with spin index $\mu \in \{x, y, z\}$; this basis will be the most convenient for our purposes.

The first term in $\mathcal{H}$ involves a sum over nearest-neighbor pairs of sites, and allows the bosons to tunnel, with 'hopping' strength t. We will restrict attention to square and cubic lattices, but the results can be straightforwardly generalized to other cases. The function $V(n)$ contains an on-site spin-independent interaction and the chemical potential; we will write it in the form

$$V(n) = \frac{1}{2} U n(n-1) - \mu n \ . \tag{3.2}$$

In the final term of Eq. (3.1), $\mathbf{L}_i$ is the total angular momentum on site i, given by (for $F = 1$) $L_{i,\rho} = -\mathrm{i}\epsilon_{\mu\nu\rho} b^\dagger_{i\mu} b_{i\nu}$, where $\epsilon_{\mu\nu\rho}$ is the completely antisymmetric tensor. For $F = 1$, this term is the most general quartic on-site spin-dependent interaction. For spin F, the boson operator becomes a tensor of rank F and there are $F + 1$ independent quartic interaction terms corresponding to different contractions of the spin indices [83]. We will not include any direct interactions between spins on neighboring sites, nor long-range polar forces between the atoms.[1]

Suppose that $V(n)$ has its minimum near some even integer, N, and the couplings are tuned so that the model is particle–hole symmetric around this filling. Requiring

[1] Note that we have also made the simplification of including only interaction terms up to fourth power in the boson operators. This neglects three-body interactions, for instance, which may be important for quantitative agreement with experiment. The analysis here can be straightforwardly extended to include such terms.

this symmetry corresponds to restricting consideration to the case of integer filling factor, and is equivalent to using the canonical ensemble [56].

3.2.2 Classification of phases

The spinless Bose-Hubbard model, with a single species of boson, has a transition from a Mott insulator when $U \gg t$ to a superfluid when $U \ll t$ [55, 56]. When the bosons have spin, various types of spin ordering are possible within both the insulator and superfluid.

With an even number of particles per site, the simplest insulating phase, the spin-singlet insulator (SSI), has a spin singlet on each site. This will be favored energetically when $J > 0$, and we will restrict to this case in the following. For $J < 0$ or odd N, the net spin on each site will be nonzero, and the system will be well described by a quantum spin model, allowing various forms of spin ordering within the lattice [65].

In a simple superfluid, the bosons condense, so that $\langle b_{i\mu} \rangle \neq 0$, breaking both gauge and spin symmetries. For $J > 0$, a so-called polar condensate[2] (PC) is favored, with $\langle b_{i\mu} \rangle \propto \delta_{\mu z}$, where z is an arbitrary direction. A variety of other condensates are, in general, also allowed [61].

For large enough J, a second variety of superfluid is possible [64], within which single bosons have not condensed. Instead, pairs of bosons condense, giving $\langle b_{i\mu} b_{i\mu} \rangle \neq 0$, which does not break spin-rotation symmetry. For this state, the spin-singlet condensate (SSC), to be energetically favorable, J must be large enough to overcome the kinetic-energy cost associated with pairing.

[2]This name was chosen [60] by analogy with the corresponding state of superfluid helium-3.

3.2.3 Continuum action

To describe the low-energy excitations of the model, we will derive a continuum field theory that captures the physics near to zero momentum. This assumes the absence of antiferromagnetic ordering of the spins, for example; it is chosen to be appropriate to the phases with which we are concerned.

The action that results is in fact completely determined by the symmetries of the model, but we will outline the steps of a formal derivation.

We first write the partition function as a path integral and decouple the hopping term using a site-dependent field ψ_μ, as with the standard (spinless) Bose-Hubbard model [55]. We then use perturbation theory in ψ_μ to eliminate all particle and hole excitations, leaving only the manifold of states with precisely N bosons per site.

The low-energy Hilbert space on each site then consists of a singlet state $|s\rangle$ and a quintet of states with $L_i = 2$, which we label $|d_m\rangle$. We use slave bosons with annihilation operators s and d_m to write these as

$$|s\rangle = s^\dagger|0\rangle \quad \text{and} \quad |d_m\rangle = d_m^\dagger|0\rangle \ , \tag{3.3}$$

where $|0\rangle$ is a fictitious vacuum state. These bosons are subject to the constraint

$$s^\dagger s + d_m^\dagger d_m = 1 \ , \tag{3.4}$$

applied on each site.

We can now make a Holstein-Primakoff expansion to eliminate s, taking into account the constraint. (For another example of this technique, see Ref. [84].) This then allows the continuum limit to be taken, assuming that all the important low

energy excitations are near zero momentum.[3] Finally, the field arising from the slave boson d_m can be integrated out to leave a field theory for ψ_μ.

The final form of the action is completely determined by the U(1) phase and SU(2) spin symmetry of the original Hamiltonian. Since the parameters have been chosen to give particle–hole symmetry, it can be written in a relativistic form:

$$\mathcal{S}_\psi = \int \mathrm{d}^d\mathbf{x}\ \mathrm{d}t\ \left(-\bar{\psi}_\mu \partial^2 \psi_\mu + r\,\bar{\psi}_\mu \psi_\mu\right) + \mathcal{S}_\psi^{(4)} + \cdots\ . \tag{3.5}$$

Note that the action is completely relativistic and the derivative ∂ acts in $D = d+1$ dimensions: $\partial^2 = \nabla^2 - \partial_t^2$. The quartic interaction contains two terms:

$$\mathcal{S}_\psi^{(4)} = \int \mathrm{d}^d\mathbf{x}\ \mathrm{d}t\ \left(\frac{u}{4}\,\bar{\psi}_\mu\psi_\mu\bar{\psi}_\nu\psi_\nu + \frac{v}{4}\,\bar{\psi}_\mu\bar{\psi}_\mu\psi_\nu\psi_\nu\right)\ . \tag{3.6}$$

The first term has full SU(3) symmetry, while the second term, which vanishes if $J = 0$ in $\mathcal{H}$, breaks this down to SU(2).

For higher spin F, the action has a similar form, with the field ψ becoming a tensor of rank F. The quadratic part of the action is unchanged, but the quartic term now involves the $F+1$ distinct scalar contractions of the field.

3.3 Mean-field theory

To provide a concrete, if qualitative, guide to the phase structure of the particular model in Eq. (3.1), we implement a mean-field theory capable of describing the phases of interest. This will be similar to the approach of Ref. [55] for the spinless

[3] One can instead take the continuum limit before eliminating s, resulting in a gauge theory. Physically, this stems from the redundancy in the slave boson description and the constraint, Eq. (3.4). The continuum action described here results from allowing s to condense, causing the gauge field to acquire a gap by the Anderson-Higgs mechanism. This field can then be integrated out, leaving an action in terms of d alone. We neglect the alternative possibility of the gauge field becoming deconfining.

Bose-Hubbard model, where a mean-field decoupling is applied to the hopping term.

3.3.1 Strong-pairing limit

Before describing the full mean-field calculation, we will first use a very simple perturbative calculation to give an approximate criterion for condensation of boson pairs. In the limit of large J/U, an odd number of bosons on any site is strongly disfavored, and we can deal with a reduced Hilbert space of singlet pairs.

The effective tunneling rate τ for such pairs is given by $\tau \sim t^2/v_1$, where $v_1 = U + 2J$ is the energy of the intermediate state with a 'broken' pair. The effective repulsion of two pairs (ie, four bosons) on the same site is $\Upsilon \sim v_2 = 4U$.

We therefore arrive at the simple criterion $zt^2 \gtrsim U(U + 2J)$ for the condensation of pairs, where z is coordination number of the lattice. This should be compared with the criterion $zt \gtrsim U + 2J$ for the condensation of single bosons [55, 56]. These two simple results will be confirmed, and the numerical prefactors determined, by the mean-field analysis that follows (see Fig. 3.1).

3.3.2 Quantum rotor operators

To simplify the calculation somewhat, we will use SO(2) quantum rotor operators $\hat{n}_i$ and $a_{i\mu}$ in place of boson operators in the mean-field calculation. These satisfy

$$[a_{i\mu}, \hat{n}_j] = \delta_{ij} a_{i\mu} \tag{3.7}$$

and

$$[a_{i\mu}, a^\dagger_{j\nu}] = 0 \ . \tag{3.8}$$

This simplification, which automatically incorporates particle–hole symmetry, is convenient but inessential. The eigenvalues of $\hat{n}_i$ are both positive and negative integers.

The full Hamiltonian, from Eq. (3.1), can be written as $\mathcal{H} = V - tT$, where V is the on-site interaction and T is the kinetic energy term. In the rotor formalism, we have

$$V = \sum_i \left[U(\hat{n}_i - N)^2 + J|\mathbf{L}_i|^2 \right] , \tag{3.9}$$

where the term involving the chemical potential has been absorbed by making the spin-independent interaction explicitly symmetric about N. For simplicity, we will take $N = 2$ in the following. In the rotor formalism, the angular momentum $\mathbf{L}_i$ is defined by its commutation relations with $a_{i\mu}$, and the kinetic term is

$$T = \sum_{\langle i,j \rangle} (a^\dagger_{i\mu} a_{j\mu} + \text{h.c.}) . \tag{3.10}$$

First, consider the case when $t = 0$. Then the Hamiltonian is simply a sum of terms acting on a single site, containing only the commuting operators $\hat{n}$ and $|\mathbf{L}|^2$. The ground state on each site, which we label $|2, L\rangle$, is therefore an eigenstate both of $\hat{n}$, with eigenvalue $N = 2$, and of $|\mathbf{L}|^2$, with eigenvalue $L(L+1)$. For positive J, the ground state is a spin singlet with $L = 0$ and the lowest-lying 'charged' excitations are triplets with $L = 1$.

3.3.3 Mean-field Hamiltonian

We will proceed by choosing a mean-field (variational) ansatz that incorporates the symmetry breaking of the phases of interest. We choose to do so by defining a mean-field Hamiltonian $\mathcal{H}_{\text{mf}}$, whose ground state will be taken as the variational ansatz.

An appropriate mean-field Hamiltonian is

$$\mathcal{H}_{\rm mf} = V - T_\psi - T_\Psi - T_\Phi \ , \tag{3.11}$$

where V is the same on-site interaction as in Eq. (3.9). T_ψ is the standard mean-field decoupling of the hopping term, generalized to the case with spin,

$$T_\psi = \sum_i \left[\psi_\mu a^\dagger_{i\mu} + \psi^*_\mu a_{i\mu} \right] \ , \tag{3.12}$$

where ψ_μ is a (c-number) constant vector, which will be used as a variational parameter. The remaining terms allow for the possibility of a spin-singlet condensate through the parameters Ψ and Φ:

$$T_\Psi = \sum_i \left[\Psi a^\dagger_{i\mu} a^\dagger_{i\mu} + \Psi^* a_{i\mu} a_{i\mu} \right] \ , \tag{3.13}$$

and

$$T_\Phi = \sum_{\langle i,j \rangle} \left[\Phi a^\dagger_{i\mu} a^\dagger_{j\mu} + \Phi^* a_{i\mu} a_{j\mu} \right] \ , \tag{3.14}$$

where the sum is over nearest-neighbor pairs within the lattice.

We now use the ground state of $\mathcal{H}_{\rm mf}$, which we denote $|{\rm mf}\rangle$, as a variational ansatz and define

$$E_{\rm mf}(\psi_\mu, \Psi, \Phi) = \langle {\rm mf} | \mathcal{H} | {\rm mf} \rangle \ , \tag{3.15}$$

which should be minimized by varying the three parameters. If this minimum occurs for vanishing values of all three parameters, then $|{\rm mf}\rangle$ breaks no symmetries and the SSI phase is favored. A nonzero value for ψ_μ at the minimum corresponds to PC, while vanishing ψ_μ but nonzero values of Ψ and/or Φ corresponds to SSC.

Since $\mathcal{H}_{\rm mf}$ contains terms (within T_Φ) that link adjacent sites, it cannot be

straightforwardly diagonalized, as in the standard mean-field theory for the spinless Bose-Hubbard model. To find the phase boundaries, however, we need to keep only terms up to quadratic order in the variational parameters, which can be found using perturbation theory.

3.3.4 Variational wavefunction

To order zero in ψ_μ, Ψ and Φ, we require the ground state of V, Eq. (3.9). Assuming $U > 0$ and $J > 0$, this is given by the simple product state

$$|\mathrm{mf}^{(0)}\rangle = \prod_j |2,0\rangle_j \ . \tag{3.16}$$

To first order, the ground state of $\mathcal{H}_{\mathrm{mf}}$ is

$$|\mathrm{mf}^{(1)}\rangle = \left(\frac{1}{v_1}T_\psi + \frac{1}{v_2}T_\Psi + \frac{1}{2v_1}T_\Phi\right)|\mathrm{mf}^{(0)}\rangle \ . \tag{3.17}$$

(If rotors were not used in place of boson operators, a similar but somewhat more complicated expression would result.) All the physics incorporated in the mean-field ansatz is visible at this order: The first term allows for a condensate of single bosons, while the last two terms allow for a condensate of spin singlets. The third term is necessary to allow these singlet pairs to move around the lattice and make the SSC phase energetically favorable.

Computing E_{mf} to quadratic order in the variational parameters (which requires

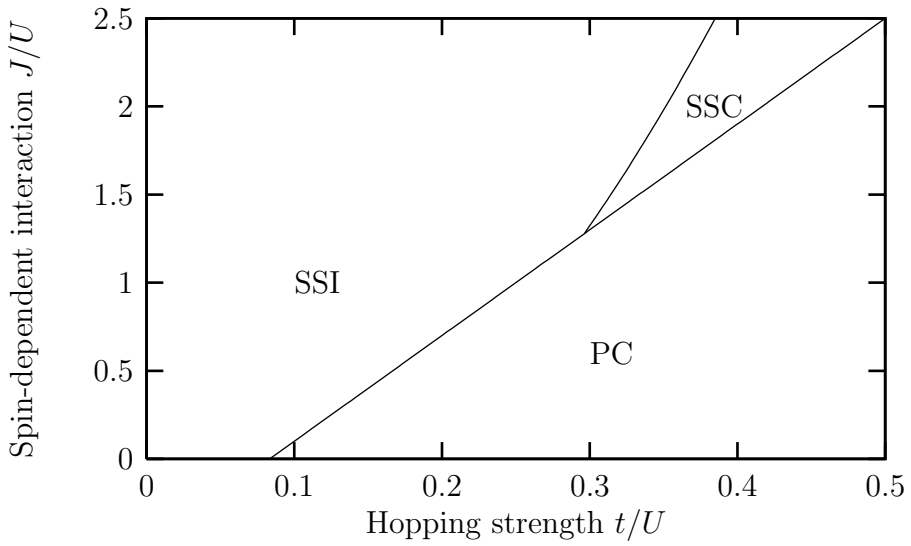

Figure 3.1: Phase diagram for the Hamiltonian in Eq. (3.1) calculated using the mean-field theory of Section 3.3. The three phases that are included are the spin-singlet insulator (SSI), the spin-singlet condensate (SSC), and the polar condensate (PC). The calculation has been performed using quantum rotors, corresponding to the canonical ensemble with the filling factor an even integer. The horizontal and vertical axes give the hopping strength t and the spin-dependent part of the interaction J, both in units of the spin-independent part of the interaction, U.

the expression for the perturbed states also to quadratic order) gives

$$E_{\mathrm{mf}} = \begin{pmatrix} \psi_\mu \\ \Psi \\ \Phi \end{pmatrix}^\dagger \begin{pmatrix} \frac{2}{v_1} - \frac{4tz}{v_1^2} & 0 & 0 \\ 0 & \frac{2}{v_2} & -\frac{9tz}{v_1 v_2} \\ 0 & -\frac{9tz}{v_1 v_2} & \frac{3z}{2v_1} \end{pmatrix} \begin{pmatrix} \psi_\mu \\ \Psi \\ \Phi \end{pmatrix} . \tag{3.18}$$

The transition to PC occurs when the top-left element in the matrix vanishes, while the transition to SSC occurs when the determinant of the remaining block vanishes. This gives the criteria $2zt > v_1$ for PC and $27zt^2 > v_1 v_2$ for SSC, in agreement with the simple considerations of Section 3.3.1. The phase boundaries are shown in Fig. 3.1.

Note that it is in fact necessary to continue the expansion to fourth order to

determine the direction of the vector ψ_μ when it is nonzero. This calculation has been performed in Ref. [85], where the possibility of SSC was not incorporated and the PC phase was found to be favored for $J > 0$, as expected.

In principle it is also necessary to continue the expansion to higher order to investigate the competition between PC and SSC in the region where both are possible. Simple energetic considerations suggest, however, that condensation of single bosons in the PC phase will dominate over condensation of pairs, and this has been assumed in Fig. 3.1.

3.4 Properties of phases

Below, in Section 3.5, we will consider the quantum phase transition from SSI to SSC. Before doing so, we first describe the low-energy properties of these two phases, based on the continuum action derived in Section 3.2.3.

The explicit calculations will be carried out in two spatial dimensions, but most of the qualitative conclusions will also apply in three dimensions.

3.4.1 Spin-singlet insulator

The SSI phase is a 'featureless' insulator without spin or phase ordering. All quasiparticle excitations are gapped, ie, they occur at finite energy above the ground state.

The phase can be further divided according to the lowest-energy 'charged' excitation. Throughout most of the phase, individual particle and hole excitations, described by the field ψ_μ, will have the smallest gap, but in a small region relatively close to the transition to SSC, bound singlet pairs will move to lower energy. (It is these excitations that condense across the transition to SSC, as described below,

in Section 3.4.3.) We will describe the former case here and return to the latter in Section 3.4.2.

In the absence of any condensate, the appropriate action is simply that given in Eq. (3.5), which we write, with $r = \lambda^2$, as

$$\mathcal{S}_{\rm SSI} = \int \mathrm{d}^d\mathbf{x}\ \mathrm{d}t\ \left[\bar{\psi}_\mu(-\partial^2 + \lambda^2)\psi_\mu + \frac{u}{4}\,\bar{\psi}_\mu\psi_\mu\bar{\psi}_\nu\psi_\nu + \frac{v}{4}\,\bar{\psi}_\mu\bar{\psi}_\mu\psi_\nu\psi_\nu + \cdots\right] . \quad (3.19)$$

Particles and holes are described by the same field ψ_μ, with gap λ and two distinct quartic interactions, with coefficients u and v.

Perturbation theory in u and v, which we take to be on the same order, will be used to describe the low-energy properties of this phase. To do so, we first define the free propagator for the field ψ_μ:

$$G_0^\psi(\omega, \mathbf{k}) = \frac{1}{-\omega^2 + k^2 + \lambda^2} . \quad (3.20)$$

Because of relativistic invariance, the results are given below for the case $\mathbf{k} = \mathbf{0}$; the corresponding expressions for nonzero momentum are given by the replacement $\omega^2 \to \omega^2 - k^2$.

Self energy

The lowest-order diagram for the self energy is the 'tadpole':

$\Sigma_1^\psi =$ 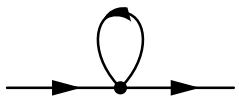 (3.21)

(where the vertex represents some linear combination of u and v). This diagram does not depend on the frequency or momentum carried by the external line and so

simply contributes a constant that renormalizes the gap λ.

The lowest-order diagram that depends on the external momentum is

$\Sigma_2^\psi =$ 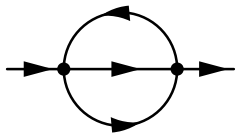 . (3.22)

The physical interpretation of this diagram is as the decay of a particle, given sufficient energy, into a hole (described by the top line, with reversed propagation direction) and two particles. It is therefore clear that this diagram will make no contribution to the decay rate for a particle unless its energy exceeds 3λ.

This interpretation is clarified by using the spectral representation; the 'spectral weight' is given by

$$\rho^\psi(\omega) = 2 \lim_{\eta \to 0^+} \operatorname{Im} G^\psi(\omega + \mathrm{i}\eta) \,, \tag{3.23}$$

where G^ψ is the full propagator. This can be calculated numerically, and is shown in Fig. 3.2.[4] There is a delta-function peak at $\omega = \lambda$ (a small width has been manually added to make it visible on the plot), and a three-body continuum, resulting from Σ_2^ψ, appears at $\omega = 3\lambda$.

3.4.2 SSI near SSC

As the spin-dependent interaction increases and the SSC phase is approached, a bound state composed of a singlet pair of bosons becomes energetically favorable. At the transition to SSC, the singlet pairs condense into a superfluid with no spin

[4]We note here a subtlety regarding this plot and those in the remainder of Section 3.4. The full series of diagrams, including those shown in Eq. (3.21) and Eq. (3.22), cause a renormalization of the gap λ (and hence movement of the features in ρ^ψ) away from its bare value, ie, the value appearing explicitly in the action. In this plot (and the ones that follow), λ should be interpreted as meaning the renormalized value, rather than the bare value, and it is for this reason that the peak appears precisely at $\omega = \lambda$.

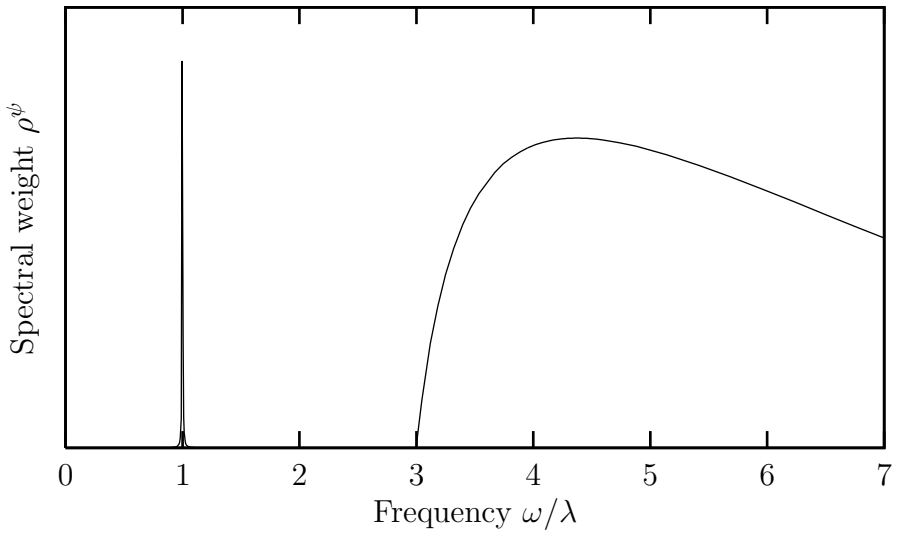

Figure 3.2: The spectral weight ρ^{ψ} in SSI, calculated up to second order in the couplings u and v. The delta-function peak at $\omega = \lambda$ (which has artificially been given a small but nonzero width) describes the stable particle excitation of the field ψ_μ. For $\omega > 3\lambda$, there is continuum of three-particle excitations.

ordering.

To describe the approach to this transition, we start with the action $\mathcal{S}_{\rm SSI}$ and introduce the field $\Psi \sim \psi_\mu \psi_\mu$, by a Hubbard-Stratonovich decoupling of the quartic interaction v. The field Ψ describes the singlet pairs and will condense across the transition. It is described by the action

$$\mathcal{S}_\Psi = \int {\rm d}^d\mathbf{x}\ {\rm d}t\ \left(|\partial\Psi|^2 + r_\Psi |\Psi|^2 + \frac{u_\Psi}{4}|\Psi|^4 + \cdots \right)\ . \tag{3.24}$$

The full action has the form

$$\mathcal{S}'_{\rm SSI} = \mathcal{S}_\psi + \mathcal{S}_\Psi + \frac{g_\psi}{2}\int {\rm d}^d\mathbf{x}\ {\rm d}t\ \left(\bar{\Psi}\psi_\mu\psi_\mu + \Psi\bar{\psi}_\mu\bar{\psi}_\mu \right)\ . \tag{3.25}$$

(The introduction of the field Ψ renormalizes the coupling constants within $\mathcal{S}_\psi$. Here and throughout, we will simplify the notation by retaining the same symbols for these

renormalized quantities.)

Self energy

The diagrams shown in Section 3.4.1, coming from $\mathcal{S}_\psi$, will still contribute to the self energy near to SSC. As seen above, however, these diagrams are important only for $\omega > 3\lambda$, whereas new diagrams coming from coupling to the pair field Ψ will contribute at lower frequencies.

Using a dashed line for the propagator of the Ψ field, the first such diagram is

$$\Sigma_1^\psi = \quad , \tag{3.26}$$

in which a particle decays into a hole plus a pair. The vertices correspond to factors of g_ψ. The threshold for this process is clearly $\lambda + \lambda_\Psi$, where λ is the gap to the particle and hole excitation as before, and $\lambda_\Psi = \sqrt{r_\Psi}$ is the gap to the pair excitation. This excitation therefore becomes important at low energies when $\lambda_\Psi < 2\lambda$, which is simply the condition that a bound state exists below the two-particle continuum.

The diagram can be evaluated to give

$$\Sigma_1^\psi = \frac{g_\psi^2}{8\pi\omega} \log \frac{\lambda + \lambda_\Psi + \omega}{\lambda + \lambda_\Psi - \omega} \, , \tag{3.27}$$

and the corresponding spectral weight is shown in Fig. 3.3. A continuum of excitations appears for $\omega > \lambda + \lambda_\Psi$, as expected. As the transition to SSC is approached, λ_Ψ becomes smaller and the edge of the continuum approaches the peak at $\omega = \lambda$. The perturbation expansion used here breaks down as $\lambda_\Psi \to 0$ and a more sophisticated RG calculation, described in Section 3.5.1, is required.

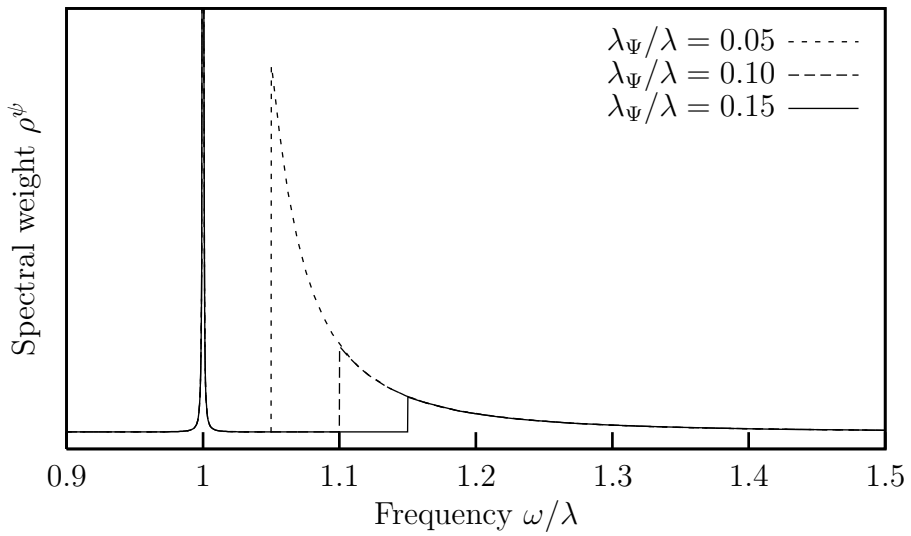

Figure 3.3: The spectral weight ρ^ψ in SSI near the transition to SSC, calculated up to order g_ψ^2, plotted for three different values of λ_Ψ, the gap to pair excitations. The coupling strength is $g_\psi = 0.1$. The peak at $\omega = \lambda$ (which is present for all values of λ_Ψ and has artificially been given a small but nonzero width) describes the stable particle and hole excitation of the field ψ_μ. For $\omega > \lambda + \lambda_\Psi$, there is continuum of excitations, corresponding physically to the conversion of a particle to a pair plus a hole.

3.4.3 Spin-singlet condensate

In the SSC phase, singlet pairs of bosons form a condensate, giving a superfluid with no spin ordering. The perturbation expansion used in Section 3.4.2 is not applicable here, and we must instead expand about the new ground state, with a condensed Ψ field. (A similar approach can be used to describe the condensed phase of the spinless Bose gas [86].)

We first write Ψ in terms of amplitude and phase as

$$\Psi = \Psi_0 \mathrm{e}^{\mathrm{i}\theta'} \ , \tag{3.28}$$

where Ψ_0 and θ' are both real. For simplicity, we treat the amplitude of the Ψ field as a constant, ignoring the gapped amplitude modes. (This is appropriate sufficiently far from the transition to SSI, where the gap is large.) With this parameterization, $\mathcal{S}_\Psi$, given by Eq. (3.24), can be rewritten as the action of a free, gapless field:

$$\mathcal{S}_\Psi = \int \mathrm{d}^d\mathbf{x}\ \mathrm{d}t\ \frac{1}{2}(\partial\theta)^2 \ , \tag{3.29}$$

with the definition $\theta = \sqrt{2}\Psi_0\theta'$. Physically, θ is interpreted as the Goldstone mode corresponding to the broken phase symmetry in SSC.

In dealing with ψ_μ, it is convenient to take out a factor of the condensate phase by writing $\psi_\mu = \varphi_\mu \mathrm{e}^{\mathrm{i}\theta'/2}$. Then, since the condensate has broken phase-rotation invariance, we rewrite the field φ_μ in terms of real and imaginary parts,

$$\varphi_\mu = \frac{1}{\sqrt{2}}(\varphi_\mu^R + \mathrm{i}\varphi_\mu^I) \ . \tag{3.30}$$

In terms of the new fields θ, φ_μ^R and φ_μ^I, the action becomes[5]

$$\begin{aligned}\mathcal{S}_{\rm SSC} = \int \mathrm{d}^d\mathbf{x}\ \mathrm{d}t \Big\{ &\frac{1}{2}(\partial\theta)^2 + \frac{1}{2}\varphi_\mu^R(-\partial^2 + r + g^\psi\Psi_0/2)\varphi_\mu^R \\ &+ \frac{1}{2}\varphi_\mu^I(-\partial^2 + r - g^\psi\Psi_0/2)\varphi_\mu^I + \frac{u}{16}\,(\varphi_\mu^R\varphi_\mu^R + \varphi_\mu^I\varphi_\mu^I)(\varphi_\nu^R\varphi_\nu^R + \varphi_\nu^I\varphi_\nu^I) \\ &+ \frac{v}{16}\,\left[(\varphi_\mu^R\varphi_\mu^R - \varphi_\mu^I\varphi_\mu^I)(\varphi_\nu^R\varphi_\nu^R - \varphi_\nu^I\varphi_\nu^I) + 4\varphi_\mu^R\varphi_\mu^I\varphi_\nu^R\varphi_\nu^I\right] \\ &+ \frac{i}{\sqrt{8}\Psi_0}(\varphi_\mu^I\partial\varphi_\mu^R - \varphi_\mu^R\partial\varphi_\mu^I)\cdot\partial\theta + \frac{1}{16\Psi_0^2}(\varphi_\mu^R\varphi_\mu^R + \varphi_\mu^I\varphi_\mu^I)(\partial\theta)^2\Big\}\ . \quad (3.31)\end{aligned}$$

Note that the two fields φ_μ^R and φ_μ^I remain gapped, but that their gaps are no longer the same. The lowest-energy 'charged' mode is φ_μ^I, with gap $\lambda_I = \sqrt{r - g^\psi\Psi_0/2}$.

Self energy

As an example, we consider the lowest-order diagram that contributes to the self energy for φ_μ^I, at energies well below that required to produce an excitation of the field φ_μ^R. This is given by

$\Sigma^\varphi =$ 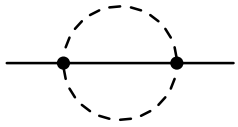 , (3.32)

where the solid lines represent φ_μ^I and the dashed lines θ. Each vertex represents a factor $\sim (p_1\cdot p_2)\Psi_0^{-2}$, where p_1 and p_2 are the momenta of the two θ propagators, coming from the final term in $\mathcal{S}_{\rm SSC}$. (All the other interaction terms involve φ_μ^R and contribute to the decay rate only at higher energies. As in Section 3.4.1, there is also a lower-order tadpole diagram that does not contribute to the decay rate.)

The diagram can be calculated numerically and the corresponding spectral weight

[5]It is straightforward to show that the Jacobian associated with the change of variables is equal to a constant.

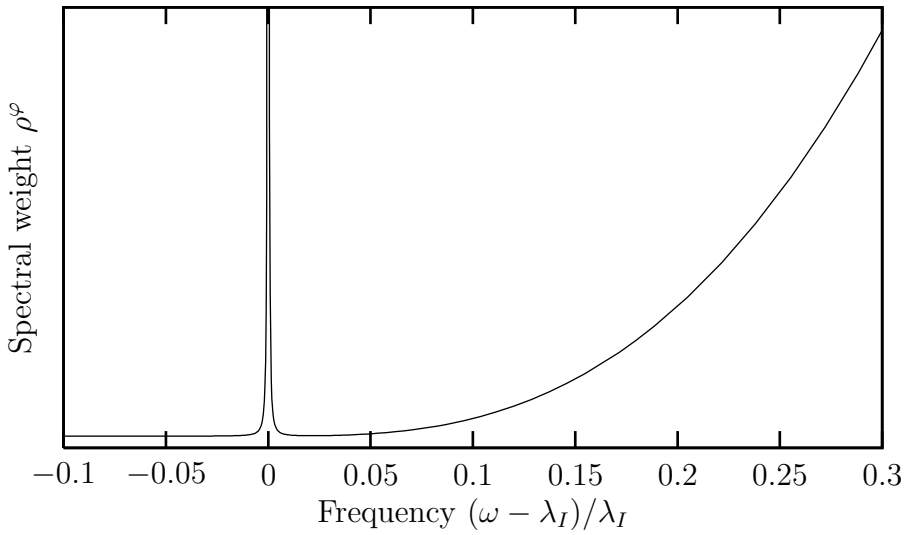

Figure 3.4: The spectral weight ρ^φ for the field φ^I_μ in SSC, near the gap λ_I, calculated numerically using the diagram in Eq. (3.32). As in Figs. 3.2 and 3.3, there is a delta-function peak at $\omega = \lambda_I$ (which has artificially been given a nonzero width), corresponding to the stable particle excitation. In this case, unlike in SSI, the continuum in the spectral weight occurs immediately above the peak. This is due to the (gapless) Goldstone mode θ resulting from the broken phase symmetry in SSC. The derivatives in the coupling between the Goldstone mode and the φ^I_μ field in $\mathcal{S}_{\rm SSC}$ strongly suppress the spectral weight as $\omega \to \lambda_I$ from above; in fact, $\rho^\varphi \sim (\omega - \lambda_I)^3$.

is shown in Fig. 3.4. As in SSI, there is a sharp peak (at $\omega = \lambda_I$) corresponding to the stable gapped 'charged' mode, followed at higher energy by a continuum of excitations. In this case, however, the Goldstone mode θ causes the continuum to begin precisely at $\omega = \lambda_I$, albeit suppressed by a factor of $(\omega - \lambda_I)^3$.

This should be contrasted with the transition between SSI and SSC, described below in Section 3.5.1. At the transition, the gapless modes are critical, rather than Goldstone modes, and their coupling is not suppressed by powers of the momentum. As a result, the spectral weight, calculated perturbatively, does not tend to zero as $\omega \to \lambda$ (see Section 3.5.2) and a RG analysis shows that the sharp peak at $\omega = \lambda$ is in fact replaced by a weaker singularity.

3.5 Critical properties

The critical field at the transition to SSC is the singlet pair Ψ, introduced in Section 3.4.2. Once Ψ has been isolated, ψ_μ, which has no gapless excitations, can be safely integrated out. This leaves the field theory of a single complex scalar, with the same form[6] as the action $\mathcal{S}_\Psi$ given in Eq. (3.24):

$$\mathcal{S}_\Psi = \int \mathrm{d}^d\mathbf{x}\ \mathrm{d}t\ \left(|\partial\Psi|^2 + r_\Psi |\Psi|^2 + \frac{u_\Psi}{4}|\Psi|^4 + \cdots \right) . \tag{3.33}$$

This transition is therefore of the XY universality class, with upper critical dimension $D = d + 1 = 4$. (The field Ψ has engineering dimension $[\Psi] = (d-1)/2$, so the coupling u_Ψ has dimension $[u_\Psi] = 3 - d$.)

While the action $\mathcal{S}_\Psi$ is sufficient to describe the critical properties of the ground state across the transition, we are also interested in the behavior single-particle excitations, and other excitations that carry spin. Since Ψ is spinless, the critical theory given by $\mathcal{S}_\Psi$ does not describe these. Instead, we must keep the singly-charged excitations given by ψ_μ, and use the full action $\mathcal{S}'_{\mathrm{SSI}}$, in Eq. (3.25).

Since ψ_μ has only gapped excitations, while the field Ψ is now gapless, this can be simplified somewhat. The important excitations are those just above the gap $\lambda = \sqrt{r}$, for which the dispersion can be replaced by a nonrelativistic form. We define particle and hole operators so that $\psi_\mu \sim p_\mu + \bar{h}_\mu$, giving an action $\mathcal{S}_\Psi + \mathcal{S}'_{\Psi,\psi}$,

[6] Integrating out the field ψ_μ renormalizes the constants in $\mathcal{S}_\Psi$. We will retain the same symbols for the renormalized quantities, because we are interested in the critical behavior, which is described by a fixed point of the action and is not dependent on the precise values of the parameters.

where

$$\mathcal{S}'_{\Psi,\psi} = \int \mathrm{d}^d\mathbf{x}\ \mathrm{d}t\ \left[\bar{p}_\mu \left(\mathrm{i}\partial_t - \frac{\nabla^2}{2m_\psi} + \lambda\right) p_\mu + \bar{h}_\mu \left(\mathrm{i}\partial_t - \frac{\nabla^2}{2m_\psi} + \lambda\right) h_\mu \right. \\ \left. + g_\psi \left(\bar{\Psi} p_\mu \bar{h}_\mu + \Psi \bar{p}_\mu h_\mu\right)\right] . \quad (3.34)$$

Using power counting (and taking $[t] = [\mathbf{x}] = -1$, since the critical theory $\mathcal{S}_\Psi$ is relativistic), the engineering dimension of the kinetic-energy term is $[1/m_\psi] = -1$. The dispersion is therefore irrelevant and the particles and holes can be treated as static impurities. This gives, finally,

$$\mathcal{S}_{\Psi,\psi} = \int \mathrm{d}^d\mathbf{x}\ \mathrm{d}t\ \left[\bar{p}_\mu \left(\mathrm{i}\partial_t + \lambda\right) p_\mu + \bar{h}_\mu \left(\mathrm{i}\partial_t + \lambda\right) h_\mu + g_\psi \left(\bar{\Psi} p_\mu \bar{h}_\mu + \Psi \bar{p}_\mu h_\mu\right)\right] . \quad (3.35)$$

The scaling dimension of the coupling g_ψ is $[g_\psi] = (3-d)/2$, so that it is relevant for $d < 3$. It is therefore relevant in two (spatial) dimensions and marginal in three, and we will consider both of these cases below. Any other interactions, including terms quartic in p_μ and h_μ, are irrelevant.

In Section 3.5.1, we will treat the case $d = 2$ using a renormalization-group (RG) analysis, and then, in Section 3.5.2, return to the case $d = 3$, where straightforward perturbation theory is sufficient.

3.5.1 Renormalization group

For $d < 3$, the correlation functions of the particle and hole excitations can be found using a RG calculation. Since the present approach is slightly different from the standard RG, we perform the calculation using a cutoff in momentum space, which makes the logic involved more transparent, in Section A.3 of the appendix. Here we use dimensional regularization, which is the simplest approach from a calculational

point of view.

We define the (imaginary-time) free propagator for the Ψ field as

$$G_0^{\Psi}(\mathbf{k}, \mathrm{i}\omega) = \frac{1}{k^2 + \omega^2 + r_\Psi} \, . \tag{3.36}$$

At the critical point, the renormalized mass of Ψ vanishes; in dimensional regularization, this occurs for $r_\Psi = 0$. For the p_μ and h_μ fields, the propagator is

$$G_0^{\psi}(\mathrm{i}\omega) = \frac{1}{-\mathrm{i}\omega + \lambda} \, , \tag{3.37}$$

independent of the momentum.

The renormalization of the terms in the action $\mathcal{S}_\Psi$ describing Ψ is identical to the standard analysis: the presence of the gapped ψ_μ excitations cannot affect the critical behavior of the gapless Ψ field. The corresponding RG has a fixed point with u_Ψ of order $\epsilon = 3 - d$, and wavefunction renormalization $Z_\Psi = 1 + \mathcal{O}(\epsilon^2)$ [87].

To lowest order in the coupling g_ψ (or, as will subsequently be shown to be equivalent, in an expansion in ϵ), the only self-energy diagram for the particle field p_μ is as shown in Eq. (3.26):

$\Sigma_1^{\psi}(\mathrm{i}\omega) =$ 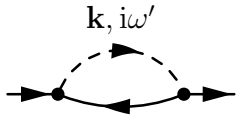

(3.38)

$$= g_\psi^2 \int_{\mathbf{k}} \int_{-\infty}^{\infty} \frac{\mathrm{d}\omega'}{2\pi} \, G_0^{\Psi}(\mathbf{k}, \mathrm{i}\omega') G_0^{\psi}\big(\mathrm{i}(\omega - \omega')\big) \, , \tag{3.39}$$

where

$$\int_{\mathbf{k}} \equiv \int \frac{\mathrm{d}^d\mathbf{k}}{(2\pi)^d} \equiv \Omega_d \int_0^{\infty} \mathrm{d}k \, k^{d-1} \tag{3.40}$$

(for an isotropic integrand). There is no diagram giving a renormalization of the

coupling g_ψ at this order, so this is the only diagram that must be evaluated.

Performing the integral over ω' using contour integration gives

$$\Sigma_1^\psi(\mathrm{i}\omega) = g_\psi^2 \int_{\mathbf{k}} \frac{1}{2k} \cdot \frac{1}{-\mathrm{i}\omega + \lambda + k} \,, \tag{3.41}$$

which leads to, defining $z = -\mathrm{i}\omega + \lambda$,

$$\Sigma_1^\psi(\mathrm{i}\omega) = -\frac{g_\psi^2 z^{1-\epsilon}}{4\pi^2\epsilon} \,, \tag{3.42}$$

plus terms that are finite as $\epsilon \to 0$.

To this order, the full propagator of the particle is then given by

$$(G^\psi)^{-1} = z - \Sigma_1^\psi \tag{3.43}$$

$$= z\left(1 + \frac{g_\psi^2 z^{-\epsilon}}{4\pi^2\epsilon}\right) \,, \tag{3.44}$$

so that renormalizing the propagator (using minimal subtraction) at real frequency $z = \mu$ gives for the wavefunction renormalization

$$Z_\psi = 1 - \frac{g_\psi^2 \mu^{-\epsilon}}{4\pi^2\epsilon} \,. \tag{3.45}$$

Since there are no diagrams corresponding to renormalization of the coupling, we have $Z_g = 1$, to this order.

We now define the (dimensionless) renormalized coupling $\tilde{g}_\psi$, given by

$$g_\psi = 2\pi\tilde{g}_\psi \frac{\mu^{\epsilon/2} Z_g}{Z_\psi \sqrt{Z_\Psi}} \,. \tag{3.46}$$

In terms of this, we have $Z_\psi = 1 - \tilde{g}_\psi^2/\epsilon$, and the beta function for the coupling is

given by

$$\beta(\tilde{g}_\psi) \equiv \mu\left(\frac{\partial \tilde{g}_\psi}{\partial \mu}\right)_{g_\psi} = \tilde{g}_\psi\left(-\frac{\epsilon}{2} + \tilde{g}_\psi^2\right) \ , \tag{3.47}$$

so that the fixed point is at

$$\tilde{g}_\psi^\star = \sqrt{\frac{\epsilon}{2}} \ . \tag{3.48}$$

Since the fixed point has $\tilde{g}_\psi^\star \sim \epsilon^{1/2}$, a perturbative expansion at this point is indeed equivalent to an expansion in ϵ.

The anomalous dimension of the particle (and hole) propagator is then given by

$$\eta_\psi = \beta \frac{\mathrm{d}}{\mathrm{d}\tilde{g}_\psi} \log Z_\psi \ , \tag{3.49}$$

so that $\eta_\psi = \epsilon/2$ at the fixed point.

We have also obtained results for the next order in this expansion [70], which also involves diagrams renormalizing the coupling g_ψ. The fixed point then occurs at

$$(\tilde{g}_\psi^\star)^2 = \frac{1}{2}\epsilon - \left(\frac{\pi^2}{15} - \frac{49}{100}\right)\epsilon^2 + \mathcal{O}(\epsilon^3) \ , \tag{3.50}$$

and the anomalous dimension is

$$\eta_\psi = \frac{1}{2}\epsilon + \left(\frac{\pi^2}{15} - \frac{6}{25}\right)\epsilon^2 + \mathcal{O}(\epsilon^3) \ . \tag{3.51}$$

The Green function behaves, for $\omega > \lambda$, as

$$G^\psi(\omega) \sim (\lambda - \omega)^{-1+\eta_\psi} \ , \tag{3.52}$$

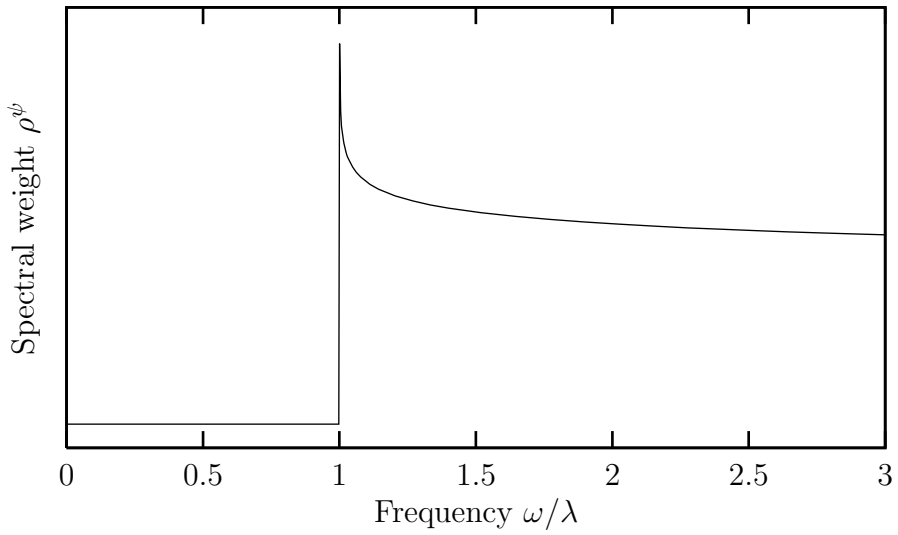

Figure 3.5: The spectral weight ρ^{ψ} at the SSI–SSC transition in $d = 2$ spatial dimensions. The delta-function peak at $\omega = \lambda$ has been replaced by a continuum of excitations, with $\rho^{\psi} \sim (\omega - \lambda)^{-1+\eta_{\psi}}$. The numerical value $\eta_{\psi} = 0.91797$ used in the plot results from a dimensional expansion in $\epsilon = 3 - d$, carried out to order ϵ^2, Eq. (3.51), and evaluated at $\epsilon = 1$.

so that the corresponding spectral weight is given by

$$\rho^{\psi}(\omega) \sim (\omega - \lambda)^{-1+\eta_{\psi}} \ . \tag{3.53}$$

The relativistic invariance of the original theory allows these results to be extended to finite external momentum by the usual replacement $\omega \to \sqrt{\omega^2 - k^2}$.

Figure 3.5 shows the spectral weight ρ^{ψ} for $d = 2$ ($\epsilon = 1$), using the numerical value from Eq. (3.51). The quasiparticle peak appearing on both sides of the critical point (see Figs. 3.2, 3.3 and 3.4) is replaced by an incoherent continuum of excitations.

Higher-order response functions

A similar calculation applies to the response functions corresponding to composite operators, such as those of the form $T_{\mu\nu}p_\mu h_\nu$. These operators, where $T_{\mu\nu}$ is an arbitrary matrix, correspond to excitations that are chargeless, but (assuming $T_{\mu\nu} \neq \delta_{\mu\nu}$) carry net spin. Such composite operators will be represented by the following 'insertion':

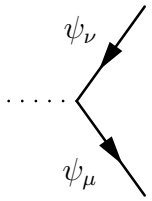

(3.54)

To find the critical exponent for these compound operators, we must consider renormalization of the corresponding insertion, given (at one-loop order) by the diagram

$H_1(2i\omega) =$ 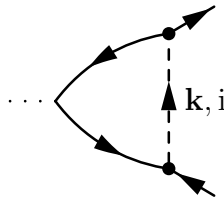

(3.55)

$$= g_\psi^2 \int_{\mathbf{k}} \int_{-\infty}^{\infty} \frac{\mathrm{d}\omega'}{2\pi} G_0^\Psi(\mathbf{k}, \mathrm{i}\omega') G_0^\psi\big(\mathrm{i}(\omega - \omega')\big) G_0^\psi\big(\mathrm{i}(\omega + \omega')\big) \,, \tag{3.56}$$

where all spin indices have been omitted. The integral can be performed to give

$$H_1(2\mathrm{i}\omega) = -\frac{g_\psi^2 z^{-\epsilon}}{4\pi^2 \epsilon} \,. \tag{3.57}$$

In accounting for the spin indices, it is important to note that the exchange of the pair interchanges the particle and hole lines and hence the indices μ and ν. This causes the results to be dependent on the symmetry of the matrix $T_{\mu\nu}$, leading to different exponents $y_{2\pm}$ for excitations of even ($T_{\mu\nu}$ symmetric) and odd spin ($T_{\mu\nu}$

antisymmetric). Including the two-loop results, we have, for the former,

$$y_{2+} = 1 - \epsilon + \left(\frac{2\pi^2}{15} - \frac{49}{50}\right)\epsilon^2 + \mathcal{O}(\epsilon^3) \ , \tag{3.58}$$

while $y_{2-} = 1$ exactly for the latter [70].

In terms of this exponent, the correlation function behaves like

$$\Pi_{\mu\nu,\rho\sigma}(2\omega) \sim (\lambda - \omega)^{-y_2} \ . \tag{3.59}$$

Of particular importance is the spectral density

$$A_{\mu\nu,\rho\sigma}(2\omega) = \lim_{\eta\to 0^+} \mathrm{Im}\, \Pi_{\mu\nu,\rho\sigma}(2\omega + \mathrm{i}\eta) \ , \tag{3.60}$$

which is a delta-function at $\omega = \lambda$ for $y_2 = 1$, and otherwise behaves like

$$A_{\mu\nu,\rho\sigma}(2\omega) \sim (\omega - \lambda)^{-y_2} \ , \tag{3.61}$$

for ω just above the gap λ.

3.5.2 Perturbation theory

For $d = 3$, the fixed point of the RG equations occurs for $\tilde{g}^\star_\psi = 0$, so perturbation theory in the coupling can be used to determine the structure of the Green function. Using the fully relativistic form of the action to calculate the lowest-order self-energy diagram gives, for $\omega^2 > \lambda^2 + k^2$,

$$\mathrm{Im}\, \Sigma^\psi_{d=3} = \frac{g^2_\psi}{8\pi} \cdot \frac{\omega^2 - k^2 - \lambda^2}{\omega^2 - k^2} \ . \tag{3.62}$$

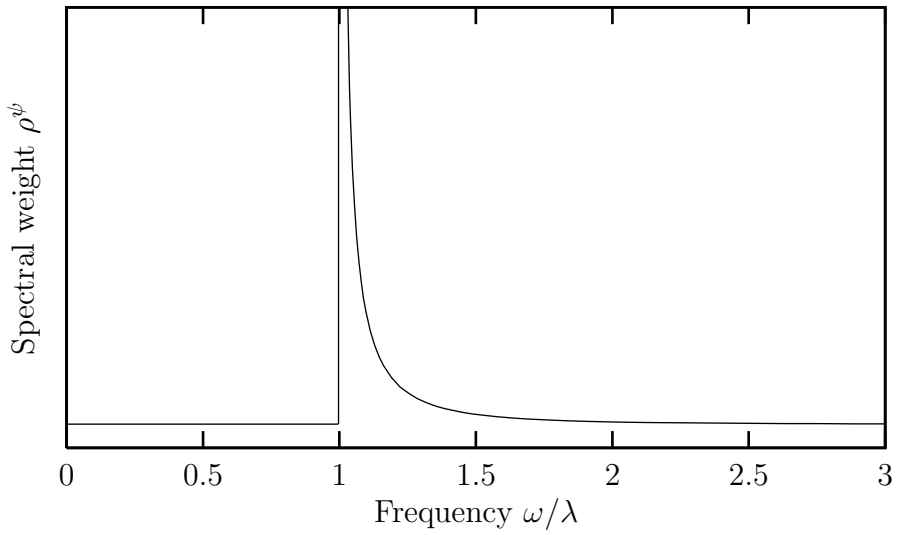

Figure 3.6: The spectral weight ρ^ψ at the SSI–SSC transition in $d = 3$ spatial dimensions. The delta-function peak at $\omega = \lambda$ has been replaced by a continuum of excitations, with the mean-field exponent $\rho^\psi \sim (\omega - \lambda)^{-1}$.

For comparison, the same calculation in two dimensions gives

$$\mathrm{Im}\,\Sigma^\psi_{d=2} = \frac{g_\psi^2}{8} \cdot \frac{1}{\sqrt{\omega^2 - k^2}} \,. \tag{3.63}$$

($\mathrm{Im}\,\Sigma^\psi = 0$ for $\omega^2 < \lambda^2 + k^2$ in both cases.) Note that $\mathrm{Im}\,\Sigma^\psi_{d=2}$ tends to a constant as $\omega \to \sqrt{\lambda^2 + k^2}$ from above, in contrast to the cases considered in Section 3.4 above. The same is not true in three dimensions, and we have

$$\mathrm{Im}\,\Sigma^\psi_{d=3} \sim \omega - \sqrt{\lambda^2 + k^2} \,. \tag{3.64}$$

The corresponding spectral weight for the particle and hole excitations is shown in Fig. 3.6. As in Fig. 3.5, the coherent quasiparticle peak is replaced by a continuum of excitations, but the exponent is given by its mean-field value: $\rho^\psi \sim (\omega - \lambda)^{-1}$.

3.6 Conclusions

In this chapter, we have considered a system of bosons with spin in a lattice potential, which can be experimentally realized using atoms trapped in an optical lattice. Using the Bose-Hubbard model, extended to the case with spin, it was argued that the system allows for both spin and phase ordering. In order to have superfluidity (phase ordering) without breaking spin-rotation symmetry, it is necessary to condense singlet pairs of bosons. Such a condensed state, referred to as the spin-singlet condensate (SSC), and, in particular, the transition to this state from the featureless spin-singlet insulator (SSI), was the main focus of the chapter.

A simple mean-field theory was constructed containing the physics of these phases, by allowing explicitly for the possibility of a condensate of singlet pairs. The phase diagram (Fig. 3.1) found by this method illustrates, as expected, that the SSC is favored for sufficiently strong spin-dependent interactions.

We then turned to the description of the SSI and SSC phases in terms of their low-energy excitations. Within the insulating phase, all excitations are gapped (ie, occur at finite energy above the ground state), whereas in the condensate a gapless Goldstone mode appears, corresponding to the broken gauge symmetry. In both phases, there is a singly-charged, spin-carrying excitation corresponding to a single particle or hole, giving an infinitely sharp peak in the spectral weight. This excitation remains gapped in the SSC, where singlet pairs of particles, rather than the individual bosons, condense.

At the transition, a calculation using the renormalization group (RG) was used to show that this sharp peak is replaced by an incoherent continuum of excitations. This results from the strong coupling to the gapless critical modes at the transition. Using scaling arguments, it was shown the dispersion of the gapped particle excitation is

irrelevant (in the RG sense) and that the corresponding response function can be found by treating it as a static impurity. The anomalous exponents were then found using a dimensional expansion.

While the analysis here has addressed the specific case of bosons with spin, it should be noted that the results regarding the critical properties can be applied directly to other paired condensates. The results rely on the existence of a gap to single-particle excitations and on particle–hole symmetry near the transition, but are otherwise quite general. In Section 4.5, we describe other examples where similar results are expected.

Chapter 4

Summary and outlook

This thesis has presented theoretical analyses of two systems that might previously have been considered purely hypothetical models, but can now potentially be realized using techniques for manipulating ultracold atoms.

In the first system, a Bose-Fermi mixture with a Feshbach resonance, a phase diagram was constructed using mean-field theory, showing how simple energetic considerations and quantum-mechanical effects allow for a variety of phases. We then demonstrated that these phases could be distinguished by their different Luttinger constraints. Techniques from quantum field theory were used to describe the transitions between the phases and to investigate the validity of the mean-field theory.

For the second system, a collection of bosons with spin confined within an optical lattice, considerations of symmetry were used to classify the various possible phases and a simple mean-field theory was constructed to serve as a guide to the phase structure in the regime of interest. We then addressed the behavior of excitations carrying spin at the appearance of a spin-singlet condensate. Considerations based on the renormalization group, and a calculation using an expansion in the spatial dimensionality, allowed the critical behavior of such excitations to be determined.

I now describe some recent related experimental results, limitations of the analysis presented above, and potential future directions for related research.

4.1 Bose-Fermi mixtures: recent experiments

In recent experiments [41], the possibility of tuning a Feshbach resonance between fermionic and bosonic atoms has been demonstrated using a mixture of potassium-40 (fermion) and rubidium-87 (boson). These experiments also provide good evidence for the formation of bound molecular states as the detuning is slowly reduced from large positive values.

Unfortunately, it appears that the scattering rate between the fermionic molecules and the residual bosonic atoms is sufficiently high that the lifetime of the molecules within the trap is extremely short. This scattering has been omitted from the analysis in Chapter 2.

It is nonetheless interesting to consider the appearance of these molecules, which occurs at the line separating '1 FS + BEC' and '2 FS + BEC' on the right-hand side of Fig. 2.3 (on p. 24). To the right of this line, molecules are absent and the loss rate of atoms is low; crossing the line causes the formation of molecules and a significant loss of atoms from the trap.

Further experiments are planned [88] to map out the boundary as a function of detuning, temperature and the relative atomic numbers. A theoretical analysis beyond mean-field and incorporating the different spatial-density profiles of the two atomic species might be necessary for closer agreement with these experiments.

4.2 Universality in quantum liquids

Recent work [25] has shown that certain properties of quantum liquids at large scattering lengths, where their behavior displays universality, can be understood in terms of renormalization group (RG) flows. An expansion in the spatial dimensionality [89], similar to that described in Section 3.5.1, can be used to give explicit expressions for the universal functions.

An analysis of the case of pairing between fermions has been carried out [25] using this dimensional expansion and another technique useful for strongly interacting systems, the '$1/N$ expansion'. It would be interesting to apply these techniques to access the universal phase diagram for Bose-Fermi mixtures.

4.3 Extensions of Luttinger's theorem in related systems

A feature of particular novelty in the Bose-Fermi mixture is the appearance of different forms of Luttinger's theorem within the different phases. As described in Chapter 2, this comes about because of the separate conservation laws governing the two species of atoms. In the absence of a BEC, all of the atoms are contained within Fermi surfaces, resulting in two separate Luttinger constraints, while the presence of a condensate eliminates one of the two.

These results can in fact be extended to other systems involving multiple species of fermions, and an example is provided by fermion pairing [90] (see also Section 1.1). In the case when the densities of the two fermion species (for example, two spin states) are unequal, a paired condensate can coexist with one or more Fermi surfaces. This case is analogous to the phases '1 FS + BEC' and '2 FS + BEC' of Chapter 2, and

a single Luttinger constraint again applies, in this case to the *difference* of the Fermi surface volumes. In the absence of condensate, the two Fermi surfaces' volumes are separately constrained, as in the phase '2 FS, no BEC'.

Another, seemingly unrelated, system to which similar considerations apply is the Kondo lattice model of the heavy-fermion compounds [91–93]. In this model, electrons in localized f orbitals interact with those of the conduction band, and two number constraints can again be formulated. The connection can be made more explicit by introducing a boson to represent hybridization between the orbitals; condensation of this boson corresponds to the standard heavy Fermi liquid with a single Luttinger constraint.

4.4 Assumption of spatial uniformity

An important simplification that we have made throughout our analysis of both models is to assume spatial uniformity, while in actual experiments, it is necessary to confine the atoms using an external trapping potential. In the case of an optical lattice, this trap is superimposed upon the lattice potential and can have significant effects, which have been studied using numerical approaches [94, 95]. The main effect is to replace the uniform insulator state by a shell structure, where regions closer to the center of the potential have higher occupation numbers than those further out.

Adding a trapping potential [31] to models formulated in the continuum (such as the Bose-Fermi mixture of Chapter 2) causes the single-particle states to cease to be pure momentum states, with relatively minor quantitative effects on the phase structure. Luttinger's theorem, however, now applies in the new single-particle basis, and the momentum-space distribution has no discontinuity. It may, however, be possible to modify the trapping potential to produce one that approximates a square

well [90], for which the single-particle states again have well-defined momentum. This would allow the Fermi surface to be seen directly in the time-of-flight measurements described in Chapter 1.

4.5 Excited-state spectra at other pairing transitions

The results found in Chapter 3 for pairing transitions of bosons with spin can also be applied, with minor modifications, to the case of fermions. It was assumed throughout, however, that single-particle excitations were gapped on both sides of the pairing transition, and so the results are not applicable to the standard BCS transition from a gapless Fermi liquid.

Instead, consider a *band* insulator, with an integer number of fermions per spin state, per site of the lattice. At sufficiently strong attractive interactions between the fermions, this state undergoes a transition into a paired condensate, which is directly analogous to the SSC of Chapter 3. In both states, the single-particle excitations remain gapped as in the bosonic case.

As can be seen in Section 3.5.1, the critical properties of the gapped excitations are determined by diagrams with only one single-particle line. The bosonic nature of that particle is therefore unimportant and the results for the Green function G^{ψ} can be applied without modification to fermions. In the case of the two-particle response functions, the same results again apply, but with the roles of symmetric and antisymmetric matrices $T_{\mu\nu}$ reversed.

Besides atoms in optical lattices, our results also apply to superfluid-insulator transition in electronic systems, provided that there is an even number of electrons per unit cell. Such a situation can arise in the cuprate compounds, with a periodic

potential generated spontaneously by charge-density-wave order. For example, recent experiments in spin ladder compounds [96] have shown that each unit cell of the 'stripe' ordering pattern contains a pair of holes. The results of Chapter 3 then predict the frequency dependence of the electron photoemission spectrum across a superfluid-insulator transition in which the charge-density wave is present on both sides of the transition [70].

4.6 Other transitions of spinful bosons in optical lattices

In Chapter 3, the phase diagram of bosons with spin in optical lattices has been investigated and shown to contain a number of phases. The transition from an insulating state to a paired superfluid was the subject of our focus, because the presence of (unbroken) spin-rotation symmetry on both sides of the transition leads to interesting response functions for operators that carry spin.

More generally, the behavior of such response functions across the transitions shown in Fig. 3.1 will depend on the order parameter governing each transition. For example, the transition between the phases SSI and PC has an order parameter carrying nonzero spin. The spin-excitation spectrum is then gapless at the critical point and the standard methods of quantum critical phenomena can be used to determine the scaling dimensions. We intend to investigate this and other cases in more detail in future work.

Appendix

A.1 Dressed molecular propagator

In Chapter 2, we have considered the many-body physics of the model defined in Section 2.2. In this section, we will consider an isolated molecule, and find an expression for the renormalized ('dressed') molecular propagator [24, 75], involving all orders in the coupling g.

A.1.1 Diagrammatic description

An isolated bosonic or fermionic atom in the vacuum is an exact eigenstate of the Hamiltonian, Eq. (2.4), since the interaction terms in $\mathcal{H}_{\text{int}}$ annihilate such a state. The same is not, however, true of a molecule, for which the process shown in Eq. (2.64), which can take place in the vacuum, produces a correction to the propagator. The dressed molecular propagator can be found using the Dyson equation, which can be written diagrammatically for this case as

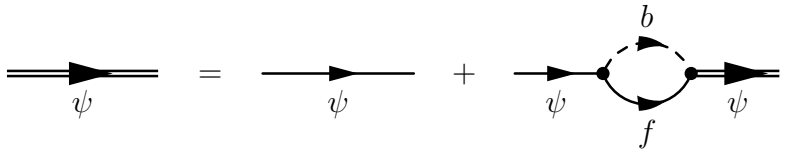

(A.1)

where only the term in the bubble diagram Eq. (2.64) of order zero in density is to be included.

A.1.2 Calculations

The Dyson equation Eq. (A.1) gives the relation between the reciprocals of the bare and full Green functions

$$\widetilde{\Xi}_q^\psi = \Xi_q^\psi - \frac{g^2}{\beta}\sum_p G_{q-p}^f G_p^b \; ; \tag{A.2}$$

compare Eq. (2.53).[1]

In the vacuum, both the Bose-Einstein and Fermi-Dirac factors give zero, leaving

$$\widetilde{\Xi}_q^\psi = \Xi_q^\psi - g^2 \int \frac{\mathrm{d}^3\mathbf{k}}{(2\pi)^3} \left(\frac{1}{\xi_{\mathbf{k}}^b + \xi_{\mathbf{k}'-\mathbf{k}}^f - \mathrm{i}\omega} - \frac{2m^f m^b}{m^\psi k^2} \right) \; , \tag{A.3}$$

where q stands for $\mathbf{k}'$ and ω, the (imaginary-time) frequency. (The second term in the parentheses comes from renormalizing the detuning ν, as in Section 2.7.1.) The integral can be performed analytically, to give

$$\widetilde{\Xi}_q^\psi = \Xi_q^\psi + 2\gamma\sqrt{\xi_{\mathbf{k}'}^\psi - \nu - \mathrm{i}\omega} \; , \tag{A.4}$$

where γ, defined in Eq. (2.7), has been used.

This function can be continued to one that is analytic everywhere except along the real axis, by replacing $\mathrm{i}\omega$ by z. In terms of z, the full Green function is

$$\widetilde{G}_{\mathbf{k}'}^\psi(z) = \frac{1}{-z + \xi_{\mathbf{k}'}^\psi + 2\gamma\sqrt{\xi_{\mathbf{k}'}^\psi - \nu - z}} \; . \tag{A.5}$$

[1] The sign difference results from the fermion loop in Eq. (2.51).

Along the real axis, the square root has a branch cut for $z > \xi^{\psi}_{\mathbf{k}'} - \nu$ which corresponds to the continuum of free-atom excitations. For $\nu < 0$, $\widetilde{G}^{\psi}$ has a single pole at the real value

$$z_0 = \xi^{\psi}_{\mathbf{k}'} - 2\gamma\left(\gamma - \sqrt{\gamma^2 - \nu}\right) \ , \tag{A.6}$$

corresponding to the renormalized molecule. For $\nu > 0$, there are no poles, since the molecule has a finite lifetime, decaying into two atoms.

A.1.3 Spectral representation

These analytical properties are best summarized using the spectral representation for $\widetilde{G}^{\psi}$,

$$\widetilde{G}^{\psi}_{\mathbf{k}'}(z) = \int_{-\infty}^{\infty} \frac{\mathrm{d}x}{2\pi} \, \frac{\rho^{\psi}_{\mathbf{k}'}(x)}{x - z} \ . \tag{A.7}$$

The spectral weight, defined in Eq. (3.23), is in this case given by

$$\begin{aligned} \rho^{\psi}_{\mathbf{k}'}(x) = \Theta(x - \xi^{\psi}_{\mathbf{k}'} + \nu) \frac{4\gamma\sqrt{x - \xi^{\psi}_{\mathbf{k}'} + \nu}}{\left(x - \xi^{\psi}_{\mathbf{k}'}\right)^2 + 4\gamma^2\left(x - \xi^{\psi}_{\mathbf{k}'} + \nu\right)} \\ + \Theta(-\nu) \frac{\sqrt{\gamma^2 - \nu} - \gamma}{\sqrt{\gamma^2 - \nu}} \, 2\pi\delta\Big(x - \xi^{\psi}_{\mathbf{k}'} - 2\gamma\big(\sqrt{\gamma^2 - \nu} - \gamma\big)\Big) \ , \end{aligned} \tag{A.8}$$

where Θ is the unit step function and δ is the Dirac delta function. A plot of $\rho^{\psi}_{\mathbf{0}}(x)$ is shown for $\gamma^2/T_0 = 2.5 \times 10^{-4}$ in Fig. A.1 and for $\gamma^2/T_0 = 0.1$ in Fig. A.2. In both cases, there is a delta-function peak at some $x < 0$ only for negative ν, and a continuum of excitations for $x > 0$ for all ν (although this is too small to be visible in Fig. A.1 for $\nu/T_0 = -1$). In the case where $\gamma^2/T_0 = 2.5 \times 10^{-4}$, there is a narrow well-defined peak in the spectral weight for $\nu > 0$, corresponding to a long-lived molecular state; it is for this reason that we refer to this case as a 'narrow' Feshbach resonance. For $\gamma^2/T_0 = 0.1$, the same peak is much broader, corresponding to a

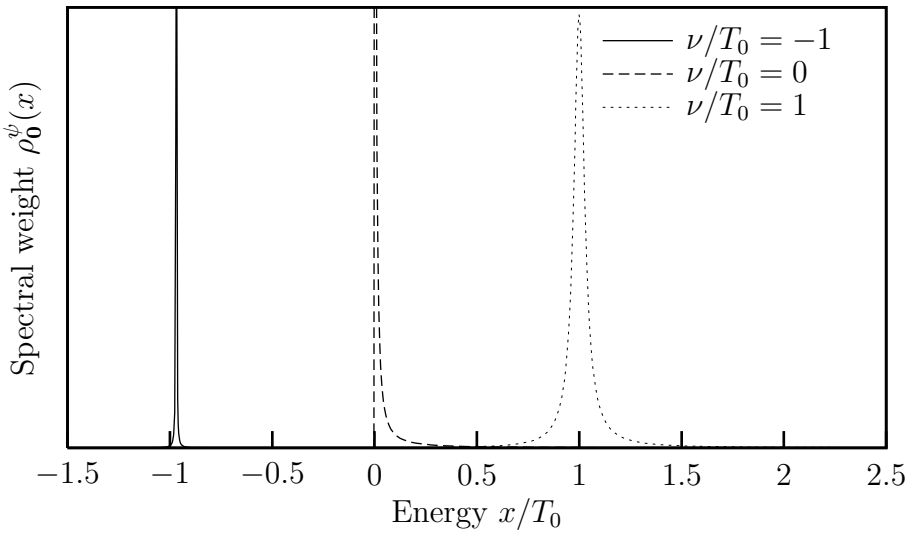

Figure A.1: The spectral weight $\rho_{\mathbf{0}}^{\psi}$ of the molecule in vacuum for a narrow Feshbach resonance, with $\gamma^2/T_0 = 2.5 \times 10^{-4}$, for three different detunings. (The density is zero in this plot, so T_0 is an arbitrarily chosen unit of energy.) The curves have all been evaluated at zero momentum; a nonzero momentum $\mathbf{k}$ would simply shift the curves to the right by an amount $k^2/(2m^{\psi})$. For $\nu < 0$, there is a delta-function peak for negative x, which has artificially been given a finite width. For all ν, there is a continuum for $x > 0$, but this is too small to be visible for $\nu/T_0 = -1$.

shorter lifetime for decay into a pair of atoms.

Note that, while the expression for $\rho_{\mathbf{k}'}^{\psi}$ depends on the momentum $\mathbf{k}'$, the latter appears only in the combination $x - \xi_{\mathbf{k}'}^{\psi}$ and we have therefore kept $\mathbf{k}' = \mathbf{0}$ for clarity. (We have similarly set $\mu^{\psi} = 0$, which in the present case simply corresponds to a choice of the zero of energy.)

Weak-coupling limit

As the coupling strength is reduced, the peak shown in Fig. A.1 for $x > 0$ and $\nu > 0$ becomes progressively narrower. In the limit $\gamma \to 0$, the first term of Eq. (A.8) involves the Lorentzian representation of the Dirac delta function,

$$\lim_{\varepsilon \to 0} \frac{\varepsilon}{t^2 + \varepsilon^2} = \pi \delta(t) \; . \tag{A.9}$$

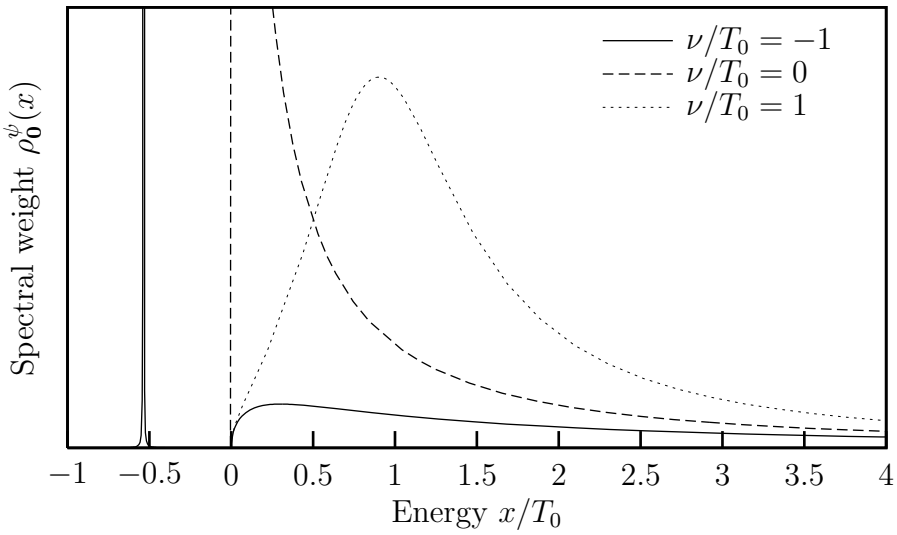

Figure A.2: As Fig. A.1, but for a broader resonance, $\gamma^2/T_0 = 0.1$.

For γ small enough, the first term of Eq. (A.8) thus has weight only near $x = \xi^{\psi}_{\mathbf{k}'}$, where $x - \xi^{\psi}_{\mathbf{k}'} + \nu$ can be replaced by ν. The limit of vanishing γ is therefore given by

$$\lim_{\gamma\to 0} \frac{2\gamma\sqrt{x - \xi^{\psi}_{\mathbf{k}'} + \nu}}{\left(x - \xi^{\psi}_{\mathbf{k}'}\right)^2 + 4\gamma^2\left(x - \xi^{\psi}_{\mathbf{k}'} + \nu\right)} = \pi\delta(x - \xi^{\psi}_{\mathbf{k}'}) \,, \tag{A.10}$$

so that the spectral weight becomes, in this limit,

$$\begin{aligned} \rho^{\psi}_{\mathbf{k}'}(x) &\to \Theta(x - \xi^{\psi}_{\mathbf{k}'} + \nu)\delta(x - \xi^{\psi}_{\mathbf{k}'}) + 2\pi\Theta(-\nu)\delta(x - \xi^{\psi}_{\mathbf{k}'}) \\ &= 2\pi\delta(x - \xi^{\psi}_{\mathbf{k}'}) \,, \end{aligned} \tag{A.11}$$

which, with Eq. (A.7), gives the free propagator for the bare molecule, as used in Section 2.6.

A.2 Stability against phase separation

The results of Chapter 2 rely on the assumption that the ground state is always a homogeneous mixture of bosons, fermions and molecules. In this section, we address the question of whether the Bose-Fermi mixture is stable to separation into multiple regions with different densities. We use the mean-field results of Section 2.4. and, for simplicity, the temperature will be taken as zero throughout.

Note that we are only allowing for instabilities allowed by the explicit model $\mathcal{H}$, given in Eq. (2.4). Other interaction terms that we have omitted may also lead to instabilities; see Section 4.1.

A.2.1 The compressibility matrix

To establish the stability of the system against separation into two coexisting fluids, we evaluate the compressibility matrix [97], defined by

$$K'_{\alpha\beta} = -\frac{\partial^2 \Phi}{\partial \mu^\alpha \partial \mu^\beta} \ , \tag{A.12}$$

for $\alpha, \beta \in \{f, b\}$.

We now define the (canonical) free energy $F(N_f, N_b)$ by a Legendre transformation,

$$F(N_f, N_b) = \Phi(\mu^f, \mu^\psi) + \mu^f N_f + \mu^b N_b \ , \tag{A.13}$$

where N_f and N_b are the total number of Fermi and Bose atoms, respectively. (Note that the full fermion and boson numbers, which are conserved by the Hamiltonian, are used.) The compressibility matrix K' is then the inverse of the Hessian of F, so that complete stability against phase separation requires that K' be positive semidefinite.

It is in fact easier to work with the matrix $K_{\alpha\beta}$, given by the same expression,

Eq. (A.12), but with $\alpha, \beta \in \{f, \psi\}$. This amounts to a simple (but not orthogonal) change of basis; it is sufficient (and necessary) for K' to be positive semidefinite that K be the same.

We begin with Eqs. (2.19) and (2.20), and use Eq. (2.26) to determine the implicit dependence of φ on the chemical potentials. We must then take second derivatives with respect to the two chemical potentials to find the compressibility matrix. In the presence of a condensate, this leads to an expression

$$K_{\alpha\beta} = K^{(0)}_{\alpha\beta} + \frac{r_\alpha r_\beta}{\tilde{\lambda}} \ , \tag{A.14}$$

where $K^{(0)}_{\alpha\beta}$ is the matrix of second derivatives, evaluated at fixed φ and r_α is a function whose form will not concern us here.

The denominator of the second term is

$$\tilde{\lambda} = \lambda + g^4 \int_{k_0^F}^{k_0^\Psi} \frac{dn(k)}{W_k^3} - \frac{1}{2} g^4 \left(z^F + z^\Psi \right) \ , \tag{A.15}$$

where

$$z^x = \left. \frac{m^\psi m^f \, \mathrm{d}n/\, \mathrm{d}k}{k \left(\xi_k^f + \xi_k^\psi \right) \left(m^f \xi_k^f + m^\psi \xi_k^\psi \right)} \right|_{k=k_0^x} \tag{A.16}$$

and

$$W_k = \sqrt{\left(\xi_k^f - \xi_k^\psi \right)^2 + 4 g^2 \varphi^2} \ . \tag{A.17}$$

When $\tilde{\lambda}$ goes through zero, the determinant of K diverges, so that the Hessian of F becomes singular, signifying that one of its eigenvalues vanishes. This marks the onset of instability; we conclude that stability requires that $\tilde{\lambda} > 0$.

When there is no condensate, such as in the phase labeled '2 FS, no BEC' in Fig. 2.3, it is found that the system is always stable.

A.2.2 Physical interpretation

The obvious physical interpretation of $\tilde{\lambda}$ is that it represents the resultant interaction between the bosons, coming partly from the explicit term λ in the Hamiltonian, Eq. (2.4), and partly from the interaction induced by coupling to the fermions. This induced interaction can alternatively be found directly by continuing the expansion in Eq. (2.48) to fourth order in b and $\bar{b}$.

A resultant interaction of the form of Eq. (A.15) is familiar from the case where the molecular degrees of freedom are not included explicitly [98,99]. This corresponds to our model for $\nu \gg 0$, when only virtual molecules are formed and the coupling term $\psi^\dagger f b$ in the Hamiltonian can be replaced by a boson–fermion scattering of the form $b^\dagger f^\dagger f b$. The induced interaction then comes from the diagram

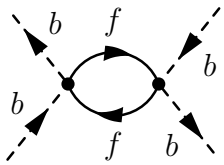

, (A.18)

which gives a term proportional to the density of states at the Fermi surface (at $T = 0$).

In this case, the induced interaction is always attractive, as can be shown by a simple physical argument. For experimentally accessible parameters, however, it is not strong enough to overcome the intrinsic repulsion between the bosons, so that the phase is stable [99]. In our notation, the boson–fermion scattering is suppressed by a factor of $1/\nu$, so that the induced interaction falls off as $1/\nu^2$. For $\nu \ll 0$, a similar picture is obtained, with the atomic and molecular fermions exchanging roles.

In the case of intermediate ν, the induced interaction is no longer so heavily suppressed, but it is also no longer the case that it is always attractive. The physical picture is clarified in this case by rewriting the action in Eq. (2.45) in terms of the

fermions F and Ψ introduced in Section 2.4.1. These fermions are defined so that there is no coupling term in the action linear in $\varphi = \langle b \rangle$; instead, the lowest order interactions have the form $\bar{F}\,\varphi^2\,F$ and $\bar{F}\,\varphi^4\,F$, and the same for Ψ. The former reproduces exactly the diagram in Eq. (A.18) above, with f replaced by F and Ψ: physically this is a boson–fermion scattering inducing an attractive interaction between the bosons, as described above. This accounts for the final term in Eq. (A.15). Note that the exclusion principle requires the momenta of the two fermion lines to be exactly at the Fermi surface, leading to z^x being evaluated at k_0^x.

The term $\bar{F}\,\varphi^4\,F$ produces the diagram

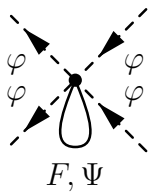

(A.19)

which also represents an induced boson–boson interaction and accounts for the integral in Eq. (A.15). Since $W_k \geq 0$, it is always repulsive and represents the fact that the fermion energy is lowered by a uniform distribution of bosons.

A.2.3 Results

The sign of the resultant interaction $\tilde{\lambda}$ must be calculated numerically to determine whether the system is indeed stable. Using the parameters from Fig. 2.3, stability is found everywhere within the plot for cases (a) and (b). In case (c), where the coupling g is larger relative to λ, there is a region of the diagram where the phase is not stable; this is shown in Fig. A.3.

For large $|\nu|$ the attractive coupling from the diagram in Eq. (A.18) is suppressed by a factor $1/\nu^2$ as described above, so that the system becomes stable. (The region for large negative ν is not visible on this plot.) For intermediate values of $|\nu|$,

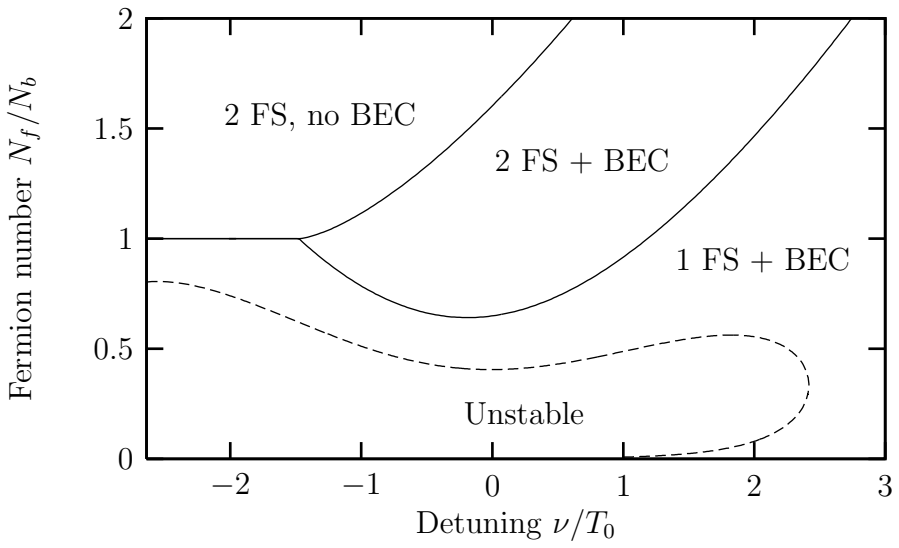

Figure A.3: The phase diagram at $T = 0$, as in Fig. 2.3, with couplings $\gamma^2/T_0 = 2.0 \times 10^{-2}$ and $\lambda^2(m^b)^3 T_0 = 2 \times 10^{-3}$. The other parameters, and the labels for the three phases, are the same as in Fig. 2.3. The region where the phase is unstable, as determined in Section A.2, is indicated.

the induced coupling becomes larger than the intrinsic coupling, λ, and it is the competition between the two diagrams in Eqs. (A.18) and (A.19) that determines the stability.

Stability is therefore favored by a higher N_f/N_b, since this increases k_0^Ψ and hence the phase space for the diagram in Eq. (A.19). The other diagram, Eq. (A.18), increases more slowly with k_0^Ψ since the internal fermion lines are restricted to be at the Fermi surface. For intermediate $|\nu|$ and very small N_f/N_b, on the order of 10^{-3}, the intrinsic interaction once more dominates the induced and the system is stable. This region is too small to be seen in Fig. A.3.

An analysis similar to that carried out in Ref. [99] could be performed to determine the stabilities of the alternative, mixed phases. It should be noted, however, that, as can be seen in Fig. A.3, the boundaries between the three phases are not disturbed at the parameters we have considered.

Furthermore, the analysis above shows that increasing the coupling g (or equivalently γ^2/T_0) beyond the value used in Fig. A.3 would increase the value of $|\nu|$ required for stability at small N_f/N_b (ie extend the unstable region to larger $|\nu|$), but would not decrease the stability at intermediate $|\nu|$. This follows from the fact that the latter is determined by the competition between the two diagrams in Eqs. (A.18) and (A.19), whose relative magnitude does not depend on g. We therefore expect that, for a broad Feshbach resonance, there remains a large region of stability for intermediate values of $|\nu|$, similar to that in Fig. A.3.

A.3 Momentum cutoff RG

In Section 3.5.1, the scaling dimensions of the particle and hole excitations across the SSI–SSC transition were found using dimensional regularization. Here, we will perform the same calculation using a momentum cutoff. (The scaling dimension of the compound operator $p_\mu h_\nu$ can be found by an analogous calculation.)

Our approach will be to calculate the correlation functions of the gapped p_μ and h_μ excitations, evaluated for real frequencies just above the gap λ. (Imaginary frequencies will be used as a formal device when calculating the diagrams, followed by analytic continuation.) We will find that there is a rescaling operation that is a symmetry of the theory and relates correlation functions evaluated at one frequency to those evaluated at another, as in a standard RG calculation. In this case, however, it is necessary to rescale relative to the gap energy λ, rather than the zero of frequency.

A.3.1 Self-energy renormalization

As a result of particle conservation, there is no one-loop diagram contributing to the renormalization of the interaction vertex.

The only one-loop diagram for the self energy of the particle (or hole) excitation is given in Eq. (3.38):

$$\Sigma_1^{\psi}(\mathrm{i}\omega) = g_{\psi}^2 \int_{\mathbf{k}} \int_{-\infty}^{\infty} \frac{\mathrm{d}\omega'}{2\pi} G_0^{\Psi}(\mathbf{k}, \mathrm{i}\omega') G_0^{\psi}\big(\mathrm{i}(\omega - \omega')\big) \;, \tag{A.20}$$

where

$$\int_{\mathbf{k}} \equiv \int \frac{\mathrm{d}^d\mathbf{k}}{(2\pi)^d} = \Omega_d \int_0^{\Lambda} \mathrm{d}k \, k^{d-1} \tag{A.21}$$

(for an isotropic integrand), with Λ the cutoff. Since the dispersion of p_μ and h_μ is irrelevant, the diagram is calculated with the external momentum equal to zero.

Working at criticality, where we set $r_\Psi = 0$, this gives

$$\Sigma_1^{\psi}(\mathrm{i}\omega) = g_{\psi}^2 \int_{\mathbf{k}} \frac{1}{2k} \cdot \frac{1}{-\mathrm{i}\omega + \lambda + k} \;, \tag{A.22}$$

after performing the integral over ω' by contour integration. With the definition $z = -\mathrm{i}\omega + \lambda$, we have

$$\Sigma_1^{\psi}(\mathrm{i}\omega) = g_{\psi}^2 \frac{\Omega_d}{2} \int_0^{\Lambda} \mathrm{d}k \, \frac{k^{d-2}}{k + z} \;. \tag{A.23}$$

Using Dyson's equation, the inverse of the propagator is therefore

$$G_1^{\psi}(\mathrm{i}\omega)^{-1} = z - \frac{g_{\psi}^2 \Omega_d}{2} \int_0^{\Lambda} \mathrm{d}k \, \frac{k^{d-2}}{k + z} + \mathcal{O}(g_{\psi}^4) \;. \tag{A.24}$$

Taking the derivative with respect to Λ and expanding in powers of z/Λ gives

$$\Lambda \frac{\partial G_1^{-1}}{\partial \Lambda} = -\frac{g_{\psi}^2 \Omega_d}{2} \Lambda^{d-2} + \frac{g_{\psi}^2 \Omega_d}{2} z \Lambda^{d-3} + \cdots \;. \tag{A.25}$$

The first term is independent of ω and so corresponds to a renormalization of λ, which is of no interest to us. The second term corresponds to wavefunction renormalization

and is the only relevant contribution from this diagram.

Since there is no diagram giving a renormalization of the coupling g_ψ, a reduction in the cutoff from Λ to $(1-\delta)\Lambda$ (with δ infinitesimal) can be compensated by replacing the action $\mathcal{S}_{\Psi,\psi}$ by

$$\mathcal{S}_{\Psi,\psi} + \delta\mathcal{S}_{\Psi,\psi} = \int \mathrm{d}^d\mathbf{x}\ \mathrm{d}\tau \left\{ \left(1+\hat{g}_\psi^2\delta\right)\left[\bar{p}_\mu\left(\partial_\tau+\lambda\right)p_\mu + \bar{h}_\mu\left(\partial_\tau+\lambda\right)h_\mu\right] + g_\psi\left(\bar{\Psi}p_\mu\bar{h}_\mu + \Psi\bar{p}_\mu h_\mu\right)\right\}. \quad \text{(A.26)}$$

To simplify this expression slightly, we have defined the dimensionless quantity[2] $\hat{g}_\psi = g_\psi\Lambda^{-(d-3)/2}\sqrt{\Omega_d/2}$.

A.3.2 Partition function

This notion of 'compensating a reduction in the cutoff' can be made more precise by considering the partition function with discrete sources:

$$\mathcal{Z}_\Lambda(J_i,\mathbf{k}_i,z_i,g_\psi) = \int_\Lambda \mathcal{D}^2p\,\mathcal{D}^2h\ \exp -\Bigg\{ \int_{\omega,\mathbf{k}} (\bar{p}_\mu z p_\mu + \bar{h}_\mu z h_\mu) + g_\psi\int_{\omega_1,\mathbf{k}_1}\int_{\omega_2,\mathbf{k}_2}\left[\bar{\Psi}(\mathbf{k}_1-\mathbf{k}_2,\mathrm{i}(\omega_1-\omega_2))p_\mu(\mathbf{k}_1,\mathrm{i}\omega_1)\bar{h}_\mu(\mathbf{k}_2,\mathrm{i}\omega_2)+\text{c.c.}\right] + \sum_i \bar{J}_{i\mu}[p_\mu(\mathbf{k}_i,\lambda-z_i)+\bar{h}_\mu(\mathbf{k}_i,\lambda-z_i)]+\text{c.c.}\Bigg\}, \quad \text{(A.27)}$$

from which correlation functions can be found by successive differentiation with respect to J_i and $\bar{J}_i$. (We are concerned with ψ_μ, so integration over Ψ, with the appropriate measure, is implied.) The subscript Λ on the integral sign denotes that a cutoff Λ should be used.

[2]Note the similarity to the corresponding definition in Eq. (3.46), since $\Omega_3^{-1} = 2\pi^2$.

Using this definition, Eq. (A.26) can be written

$$\mathcal{Z}_\Lambda(J_i, z_i, g_\psi) = \int_{(1-\delta)\Lambda} \mathcal{D}^2 p\, \mathcal{D}^2 h\, \exp -\Big\{ \left(1 + \hat{g}_\psi^2 \delta\right) \int_{\omega,\mathbf{k}} (\bar{p}_\mu z p_\mu + \bar{h}_\mu z h_\mu) + g_\psi \iint_{\omega,\mathbf{k}} \left(\bar{\Psi} p_\mu \bar{h}_\mu + \text{c.c.}\right) + \sum_i \bar{J}_{i\mu} [p_\mu(\lambda - z_i) + \bar{h}_\mu(\lambda - z_i)] + \text{c.c.} \Big\} , \quad \text{(A.28)}$$

which expresses the fact that the partition function, and hence all correlators, are unchanged by a shift in the cutoff and a compensating change in the action. A condensed notation has been used, where the momentum dependence is suppressed throughout.

To bring this closer to the form of Eq. (A.27), we rescale the fields p_μ and h_μ within the functional integral. By doing so, we can return the coefficient of the quadratic term to unity, giving

$$\mathcal{Z}_\Lambda(J_i, z_i, g_\psi) = \int_{(1-\delta)\Lambda} \mathcal{D}^2 p\, \mathcal{D}^2 h\, \exp -\Big\{ \int_{\omega,\mathbf{k}} (\bar{p}_\mu z p_\mu + \bar{h}_\mu z h_\mu) + g_\psi \left(1 - \hat{g}_\psi^2 \delta\right) \iint_{\omega,\mathbf{k}} \left(\bar{\Psi} p_\mu \bar{h}_\mu + \text{c.c.}\right) + \sum_i \left(1 - \frac{\hat{g}_\psi^2}{2}\delta\right) J_{i\mu} [p_\mu(\lambda - z_i) + \bar{h}_\mu(\lambda - z_i)] + \text{c.c.} \Big\} . \quad \text{(A.29)}$$

By comparison with Eq. (A.27), we can write

$$\mathcal{Z}_\Lambda(J_i, \mathbf{k}_i, z_i, g_\psi) = \mathcal{Z}_{(1-\delta)\Lambda}\big((1 - \hat{g}_\psi^2 \delta/2) J_i, \mathbf{k}_i, z_i, (1 - \hat{g}_\psi^2 \delta) g_\psi\big) . \quad \text{(A.30)}$$

A.3.3 Rescaling

To return to the original theory, with cutoff Λ, we now perform a rescaling of all variables according to their engineering dimensions, with $[\tau] = [\mathbf{x}] = -1$. Since we

are working at the critical point of Ψ, we have

$$\Psi(\mathbf{x}/b, \tau/b) = b^X \Psi(\mathbf{x}, \tau) \ , \tag{A.31}$$

where X is the scaling dimension of the field Ψ. By dimensional analysis of Eq. (3.33), the engineering dimension of Ψ is seen to be $[\Psi] = (D-2)/2 = (d-1)/2$ and one would naively expect $X = [\Psi] = 1 - \frac{\epsilon}{2}$. This expectation actually happens to be correct (to order ϵ), since there is no wavefunction renormalization of $\mathcal{S}_\Psi$ to one-loop order.

Performing this rescaling leads to

$$\mathcal{Z}_\Lambda(J_i, \mathbf{k}_i, z_i, g_\psi) = \mathcal{Z}_{b\Lambda}(b^{1+d/2} J_i, b\mathbf{k}_i, bz_i, b^{1-X} g_\psi) \ , \tag{A.32}$$

after making the substitutions $\psi'(\mathbf{k}, \lambda - z) = b^{d/2+1}\psi(b\mathbf{k}, \lambda - bz)$ and $\lambda - \mathrm{i}\omega' = (\lambda - \mathrm{i}\omega)/b$.

This can now be combined with Eq. (A.30) to give

$$\begin{aligned}\mathcal{Z}_\Lambda(J_i, \mathbf{k}_i, z_i, g_\psi) = \mathcal{Z}_\Lambda\big((1 - \hat{g}_\psi^2\delta/2)[1 + (1 + d/2)\delta]J_i, (1+\delta)\mathbf{k}_i, (1+\delta)z_i, \\ (1 - \hat{g}_\psi^2\delta)[1 + (1-X)\delta]g_\psi\big) \ .\end{aligned} \tag{A.33}$$

This gives a relationship between correlators in the same theory but at different frequencies.

The fixed point of Eq. (A.33) occurs when

$$g_\psi^\star = [1 - (\hat{g}_\psi^\star)^2\delta][1 + (1-X)\delta]g_\psi^\star \ , \tag{A.34}$$

so that

$$\hat{g}_\psi^\star = \sqrt{1-X} = \sqrt{\frac{\epsilon}{2}}\,, \tag{A.35}$$

which should be compared with Eq. (3.48).

A.3.4 Renormalized propagator

At the fixed point, Eq. (A.33) becomes

$$\mathcal{Z}_\Lambda(J_i, \mathbf{k}_i, z_i, g_\psi^\star) = \mathcal{Z}_\Lambda\big((1+y\delta)J_i, (1+\delta)\mathbf{k}_i, (1+\delta)z_i, g_\psi^\star\big)\,, \tag{A.36}$$

where $y = 1 + d/2 - (\hat{g}_\psi^\star)^2/2 = 5/2 - 3\epsilon/4$. Taking derivatives with respect to J_μ and $\bar{J}_\nu$ gives

$$\begin{aligned}&\big\langle \bar{\psi}_\mu(\mathbf{k}_1, \lambda - z_1)\psi_\nu(\mathbf{k}_2, \lambda - z_2)\big\rangle = \\ &\qquad (1+2y\delta)\big\langle \bar{\psi}_\mu\big((1+\delta)\mathbf{k}_1, \lambda - (1+\delta)z_1\big)\psi_\nu\big((1+\delta)\mathbf{k}_2, \lambda - (1+\delta)z_2\big)\big\rangle\,.\end{aligned} \tag{A.37}$$

Using the conservation of frequency and momentum, we can define the propagator G^ψ by

$$\big\langle \bar{\psi}_\mu(\mathbf{k}_1, \lambda - z_1)\psi_\nu(\mathbf{k}_2, \lambda - z_2)\big\rangle = (2\pi)^{d+1}\delta^d(\mathbf{k}_1 - \mathbf{k}_2)\delta(z_1 - z_2)\delta_{\mu\nu}G^\psi(\mathbf{k}_1, \lambda - z_1)\,. \tag{A.38}$$

Using this definition, Eq. (A.37) becomes

$$G^\psi(\mathbf{k}, \lambda - z) = (1 + y'\delta)G^\psi\big((1+\delta)\mathbf{k}, \lambda - (1+\delta)z\big)\,, \tag{A.39}$$

with $y' = 2y - d - 1 = 1 - \epsilon/2$.

Restricting attention to $\mathbf{k} = \mathbf{0}$ gives

$$G^{\psi}(\mathbf{0}, \lambda - z) = (1 + y'\delta) G^{\psi}\mathbf{(0}, \lambda - (1 + \delta)z\mathbf{)} \ , \tag{A.40}$$

which can be iterated to give $G^{\psi}(\mathbf{0}, \lambda - z) \sim z^{-1+\epsilon/2}$. Equivalently, after analytic continuation to real frequencies, we have

$$G^{\psi}(\mathbf{0}, \omega) \sim (\lambda - \omega)^{-1+\epsilon/2} \ , \tag{A.41}$$

which agrees with Eq. (3.52).

Bibliography

[1] M. H. Anderson, J. R. Ensher, M. R. Matthews, C. E. Wieman, and E. A. Cornell, Science **269**, 198 (1995).

[2] S. N. Bose, Z. Phys. **26**, 178 (1924).

[3] A. Einstein, Sitzungsber. Kgl. Preuss. Akad. Wiss. **1924**, 261 (1924).

[4] A. Einstein, Sitzungsber. Kgl. Preuss. Akad. Wiss. **1925**, 3 (1925).

[5] C. J. Pethick and H. Smith, *Bose-Einstein Condensation in Dilute Gases* (Cambridge University Press, Cambridge, 2001).

[6] L. P. Pitaevskii and S. Stringari, *Bose-Einstein Condensation* (Clarendon Press, Oxford, 2003).

[7] F. London, Nature **141**, 643 (1938).

[8] F. London, Phys. Rev. **54**, 947 (1938).

[9] O. Penrose and L. Onsager, Phys. Rev. **104**, 576 (1956).

[10] F. Dalfovo, S. Giorgini, L. P. Pitaevskii, and S. Stringari, Rev. Mod. Phys. **71**, 463 (1999).

[11] J. O. Andersen, Rev. Mod. Phys. **76**, 599 (2004).

[12] K. B. Davis *et al.*, Phys. Rev. Lett. **75**, 3969 (1995).

[13] E. A. Cornell and C. E. Wieman, Rev. Mod. Phys. **74**, 875 (2002).

[14] K. T. Hecht, *Quantum Mechanics* (Springer, New York, 2000).

[15] E. Altman, E. Demler, and M. D. Lukin, Phys. Rev. A **70**, 013603 (2004).

[16] J. Anglin and W. Ketterle, Nature **416**, 211 (2002).

[17] I. Bloch, J. Phys. B: At. Mol. Opt. Phys. **38**, S629 (2005).

[18] D. Jaksch and P. Zoller, Ann. Phys. **315**, 52 (2005).

[19] M. Lewenstein *et al.*, cond-mat/0606771, unpublished.

[20] H. Feshbach, Ann. Phys. **19**, 287 (1962).

[21] W. C. Stwalley, Phys. Rev. Lett. **37**, 1628 (1976).

[22] E. Tiesinga, B. J. Verhaar, and H. T. C. Stoof, Phys. Rev. A **47**, 4114 (1993).

[23] S. Inouye *et al.*, Nature **392**, 151 (1998).

[24] R. A. Duine and H. T. C. Stoof, Phys. Rep. **396**, 115 (2004).

[25] P. Nikolic and S. Sachdev, cond-mat/0609106, unpublished.

[26] J. J. Sakurai, *Modern Quantum Mechanics* (Addison Wesley, 1994).

[27] M. Greiner, C. A. Regal, and D. S. Jin, Nature (London) **426**, 537 (2003).

[28] S. Jochim *et al.*, Science **302**, 2101 (2003).

[29] M. W. Zwierlein *et al.*, Phys. Rev. Lett. **91**, 250401 (2003).

[30] C. A. Regal, M. Greiner, and D. S. Jin, Phys. Rev. Lett. **92**, 040403 (2004).

[31] G. Bruun, Y. Castin, R. Dum, and K. Burnett, Eur. Phys. J. D **7**, 433 (1999).

[32] M. Greiner, C. A. Regal, and D. S. Jin, Phys. Rev. Lett. **94**, 070403 (2005).

[33] C. A. Regal, M. Greiner, S. Giorgini, M. Holland, and D. S. Jin, Phys. Rev. Lett. **95**, 250404 (2005).

[34] Y. Ohashi and A. Griffin, Phys. Rev. Lett. **89**, 130402 (2002).

[35] Y. Ohashi and A. Griffin, Phys. Rev. A **67**, 033603 (2003).

[36] V. Gurarie and L. Radzihovsky, cond-mat/0611022, unpublished.

[37] L. Radzihovsky, J. Park, and P. B. Weichman, Phys. Rev. Lett. **92**, 160402 (2004).

[38] M. W. J. Romans, R. A. Duine, S. Sachdev, and H. T. C. Stoof, Phys. Rev. Lett. **93**, 020405 (2004).

[39] S. Inouye *et al.*, Phys. Rev. Lett. **93**, 183201 (2004).

[40] C. A. Stan, M. W. Zwierlein, C. H. Schunck, S. M. F. Raupach, and W. Ketterle, Phys. Rev. Lett. **93**, 143001 (2004).

[41] M. Zaccanti *et al.*, cond-mat/0606757, unpublished.

[42] A. G. Truscott, K. E. Strecker, W. I. McAlexander, G. B. Partridge, and R. G. Hulet, Science **291**, 2570 (2001).

[43] F. Schreck *et al.*, Phys. Rev. Lett. **87**, 080403 (2001).

[44] P. O. Fedichev, Y. Kagan, G. V. Shlyapnikov, and J. T. M. Walraven, Phys. Rev. Lett. **77**, 2913 (1996).

[45] M. Theis *et al.*, Phys. Rev. Lett. **93**, 123001 (2004).

[46] A. Hemmerich and T. W. Hänsch, Phys. Rev. Lett. **70**, 410 (1993).

[47] T. Müller-Seydlitz *et al.*, Phys. Rev. Lett. **78**, 1038 (1997).

[48] D. Jaksch, C. Bruder, J. I. Cirac, C. W. Gardiner, and P. Zoller, Phys. Rev. Lett. **81**, 3108 (1998).

[49] M. Greiner, O. Mandel, T. Esslinger, T. W. Hänsch, and I. Bloch, Nature **415**, 39 (2002).

[50] M. V. Fedorov, *Atomic and Free Electrons in a Strong Light Field* (World Scientific, River Edge, 1997).

[51] L. Santos *et al.*, Phys. Rev. Lett. **93**, 030601 (2004).

[52] G. H. Wannier, Phys. Rev. **77**, 432 (1960).

[53] J. M. Ziman, *Principles of the Theory of Solids* (Cambridge University Press, Cambridge, 1972).

[54] J. Hubbard, Proc. Roy. Soc. A **276**, 238 (1963).

[55] M. P. A. Fisher, P. B. Weichman, G. Grinstein, and D. S. Fisher, Phys. Rev. B **40**, 546 (1989).

[56] S. Sachdev, *Quantum Phase Transitions* (Cambridge University Press, Cambridge, 1999).

[57] J. K. Chin *et al.*, cond-mat/0607004, unpublished.

[58] D. M. Stamper-Kurn *et al.*, Phys. Rev. Lett. **80**, 2027 (1998).

[59] T. Ohmi and K. Machida, J. Phys. Soc. Jpn. **67**, 1822 (1998).

[60] T.-L. Ho, Phys. Rev. Lett. **81**, 742 (1998).

[61] R. Barnett, A. Turner, and E. Demler, cond-mat/0607253, unpublished.

[62] H. Pu, C. K. Law, S. Raghavan, J. H. Eberly, and N. P. Bigelow, Phys. Rev. A **60**, 1463 (1999).

[63] L. E. Sadler, J. M. Higbie, S. R. Leslie, M. Vengalattore, and D. M. Stamper-Kurn, cond-mat/0605351, unpublished.

[64] E. Demler and F. Zhou, Phys. Rev. Lett. **88**, 163001 (2002).

[65] A. Imambekov, M. Lukin, and E. Demler, Phys. Rev. A **68**, 063602 (2003).

[66] S. Tsuchiya, S. Kurihara, and T. Kimura, Phys. Rev. A **70**, 043628 (2004).

[67] D. Rossini, M. Rizzi, G. D. Chiara, S. Montangero, and R. Fazio, J. Phys. B: At. Mol. Opt. Phys. **39**, S163 (2006).

[68] L. Zawitkowski, K. Eckert, A. Sanpera, and M. Lewenstein, cond-mat/0603273, unpublished.

[69] S. Powell, S. Sachdev, and H. P. Büchler, Phys. Rev. B **72**, 024534 (2005).

[70] S. Powell and S. Sachdev, cond-mat/0608611, unpublished.

[71] H. Yabu, Y. Takayama, and T. Suzuki, Physica B **329–333**, 25 (2003).

[72] N. N. Bogoliubov, J. Phys. (Moscow) **11**, 23 (1947).

[73] J. M. Luttinger and J. C. Ward, Physical Review **118**, 1417 (1960).

[74] M. Potthoff, Condensed Matter Physics **9**, 557 (2006), cond-mat/0406671.

[75] A. A. Abrikosov, L. P. Gorkov, and I. E. Dzyaloshinski, *Methods of Quantum Field Theory in Statistical Physics* (Dover Publications Inc., New York, 1975).

[76] J. A. Hertz, Phys. Rev. B **14**, 1165 (1976).

[77] A. J. Millis, Phys. Rev. B **48**, 7183 (1993).

[78] M. Y. Kagan and D. V. Efremov, Phys. Rev. B **65**, 195103 (2002).

[79] R. Bendjama, B. Kumar, and F. Mila, Phys. Rev. Lett. **95**, 110406 (2005).

[80] J. Bardeen, L. N. Cooper, and J. R. Schrieffer, Phys. Rev. **108**, 1175 (1957).

[81] S. Sachdev, M. Troyer, and M. Vojta, Phys. Rev. Lett. **86**, 2617 (2001).

[82] S. Sachdev, Physica C **357**, 78 (2001).

[83] C. Zemach, Phys. Rev. **140**, B97 (1965).

[84] E. Altman and A. Auerbach, Phys. Rev. Lett. **89**, 250404 (2002).

[85] S. T. S. Kurihara and T. Kimura, Phys. Rev. A **70**, 043628 (2004).

[86] V. N. Popov, *Functional Integrals and Collective Excitations* (Cambridge University Press, Cambridge, 1988).

[87] J. Zinn-Justin, *Quantum Field Theory and Critical Phenomena* (Oxford University Press, Oxford, 1993).

[88] G. Modugno, personal communication.

[89] Y. Nishida and D. T. Son, cond-mat/0607835, unpublished.

[90] S. Sachdev and K. Yang, Phys. Rev. B **73**, 174504 (2006).

[91] T. Senthil, S. Sachdev, and M. Vojta, Phys. Rev. Lett. **90**, 216403 (2003).

[92] M. V. T. Senthil and S. Sachdev, Phys. Rev. B **69**, 035111 (2004).

[93] P. Coleman, I. Paul, and J. Rech, Phys. Rev. B **72**, 094430 (2005).

[94] G. G. Batrouni *et al.*, Phys. Rev. Lett. **89**, 117203 (2003).

[95] V. A. Kashurnikov, N. V. Prokof'ev, and B. V. Svistunov, Phys. Rev. A **66**, 031601 (2002).

[96] A. Rusydi *et al.*, cond-mat/0604101, unpublished.

[97] K. Huang, *Statistical Mechanics* (Wiley, New York, 1987).

[98] H. P. Büchler and G. Blatter, Phys. Rev. A **69**, 063603 (2004).

[99] L. Viverit, C. J. Pethick, and H. Smith, Phys. Rev. A **61**, 053605 (2000).